# Rate Prediction Tool Assessment for Single Event Transient Errors on Optical Link Receivers and Optocouplers

**Prepared by:**
**Paul W. Marshall**
**For NASA/Goddard Space Flight Center**

**Reviewed by:**
**Jet Propulsion Laboratory**
**Defense Threat Reduction Agency**

**For:**

**NASA Electronic Parts and Packaging (NEPP) Program**
**Electronics Radiation Characterization (ERC) Project**

**And**

**Defense Threat Reduction Agency**

**Date:**
**3/28/02**

# Task on Photonic Technology: Rate Prediction Tool Assessment for Single Event Transient Errors on Optical Link Receivers and Optocouplers

*Executive Summary:* Fiber optic link receivers and high bandwidth optocouplers share the unique distinction of exhibiting sensitivity to errors arising due to proton induced ionization. This can occur from both direct and nuclear interaction related indirect mechanisms, but in regimes where direct ionization occurs, this effect can dominate the error rate by orders of magnitude. This document reviews the published literature to assess the underlying mechanisms and our ability to predict error rates based on test data and/or detailed circuit knowledge. Existing methods and tools for assessing error and event rates in microelectronics and in imaging sensors are assessed for their applicability to this problem, and recommendations are made for adapting existing tools to the problem of rate predication with the long term goal of developing a common tool that could be used for both fiber optic links and optocouplers. Cautions are offered and error ranges suggested for application of existing tools such as CRÈME-96, and recommendations are made to utilize modern Monte Carlo approaches such as GIANT-4.

Prepared by Paul Marshall under the NASA-GSFC Multi-Engineering Disciplinary Support Contract Tasks 370 and 637

This work is sponsored by the NASA Electronic Parts and Packaging (NEPP) Program's Electronics Radiation Characterization (ERC) Project and the Defense Threat Reduction Agency's (DTRA) Radiation Hardened Microelectronics (RHM) Program

# Task on Photonic Technology: Rate Prediction Tool Assessment for Single Event Transient Errors on Optical Link Receivers and Optocouplers

## Table of Contents

## 1.0 Introduction and General Statement of Problem:

Optocouplers and fiber optic links (FOLs) both operate on the principle that light can be emitted, transmitted, and absorbed by a semiconductor to communicate signals optically. In the case of the fiber optic data link, the advantages for satellite applications include the ability to transmit very high bandwidth data streams over light weight, and electromagnetically insensitive, optical fiber with additional savings in power consumption and integration ease [1]. Optocouplers are used primarily to provide electrical isolation between microelectronic circuits by using a variation of the same basic transmit/receive architecture to transfer signals optically. Figure 1 shows schematic representations of the two basic architectures and illustrates their similarities.

While the FOL is used for box-to-box communication and local area network topologies on satellites, the optocoupler implements the optical link and isolation function within a single package. Obviously, the two differ considerably in complexity. FOL implementations may leverage on Commercial Off The Shelf (COTS) technologies, but typically undergo very careful design cycles with detailed understanding of component and subsystem radiation performance. Optocouplers, on the other hand, are strictly COTS devices, and the design engineer more often has little insight into the internal hybrid elements and details of their response to radiation. The extensive variability of optocoupler technologies and problems associated with characterizing their response for proton environments have been treated in [2,3].

In recent years, the sensitivities of both fiber optic data links and optocouplers have been examined in sufficient detail to suggest that on-orbit rate predictions can be useful, and in some cases agreement between flight observations and prediction is good. In general, however, the level of confidence that should be placed on a given rate prediction is unknown. To date, although there are obvious similarities in the fundamental issues, there is no clear agreement on test needs and rate prediction approaches that encompass both technologies. Our study examines the suggested approaches and combines a review of literature data with some new measurements to examine the possibility that a single rate prediction approach may suffice for both cases. We also consider the associated test issues and the requirements for data to support the candidate predictive methods, and assess technology related issues that impact the applicability and precision of extensions of existing tools (e.g. CRÈME-96, NOVICE, and others).

The tools under review for this relatively recent problem have been generated for other needs including Single Event Effects in microelectronics and energy and dose deposition due to nuclear reaction induced damage and transient signals in detectors for the particle physics community. As part of our study, we will provide a brief discussion of the suitability of existing tools to assess event rates and transient signatures in materials and structures found in other satellite optical detection applications such as imaging, photometric observations, spectroscopy, and others.

## 2.0 Physical Mechanisms of Particle Induced Transient Effects:

2.1 Fiber Optic Link Receivers: For both optocouplers and FOLs, the single event error mechanisms are fundamentally different from conventional microelectronics. In both cases, the most SEE sensitive element is usually the optoelectronic photodetector that captures the optical signal and generates a corresponding electrical signal as depicted in Figures 1a and 1b. The problem is exacerbated by the fact that detector elements are often large area diode structures with diameters of several hundred microns. This sensitivity was first described in optical data links by LaBel, et al. [4,5] and later in optocouplers by LaBel, et al. [6]. Additional studies of FOL sensitivities by multiple groups have confirmed the role of the photodetector [7,8],

suggested hardening solutions [8-10], and examined test needs and rate prediction strategies [8,11].

The extreme sensitivity of the photodetector is perhaps not so surprising in view of the fact that this optoelectronic detector functions to capture digital information at rates into the Gbps regime from optical signals with average powers of a few μW. The corresponding electrical signal of a few hundred or thousand electrons that represents a single bit may be easily corrupted by even lightly ionizing particles that strike the photodetector element and produce photocurrents that are indistinguishable from "valid" optical stimulus. Also, the photodiode must necessarily be large enough to capture the optical signal. For typical multimode fiber, this corresponds to surface areas of thousands of square microns (the device examined in our study has a 75 micron optical aperture with an 80 micron diameter junction). Photodiode physical cross-sections can easily exceed $10^{-5}$ $cm^2$, and in cases of extreme sensitivity, the error cross-sections can be correspondingly large.

Figure 2 depicts the disk-shaped planar photodiode structure under reverse bias conditions and indicates various particle trajectories which deposit charge by direct ionization. The sketch beneath shows resulting current pulses sensed in the receiver circuit which decay with an RC time constant determined by the circuit bandwidth. Also depicted is the received no-return-to-zero (NRZ) signal containing the digital information. The ratio between the high and low current levels, the extinction ratio, is typically about 10. Receiver circuits are almost always designed to accommodate a range of incident average optical powers and automatically adjust the decision level, or threshold, to be midway between the high and low levels. As suggested in the figure, data can be disrupted if ion-induced current exceeding the threshold current is sensed at the critical mid-bit decision when a "0" is being transmitted.

The two distributions shown at the lower right of the figure indicate the contributions of multiple noise sources leading to a distribution of signals received to represent "1s" and "0s". Except for very low incident optical signals, the shape is approximately Gaussian, though the widths have been exaggerated in the sketch. According to communications decision theory, we would expect a usually small but finite probability of false bits from the intersymbol interference where the distribution tails extend beyond the decision level. Thus *any* ion-induced photocurrent flowing when a "0" has been transmitted increases the probability of false detection. This statistical superposition of impulse noise from the particle strike with the random noise sources affecting intersymbol interference is more a concern for operation near the maximum sensitivity of the receiver circuit, and at higher incident optical powers the intersymbol interference effects on bit error ratio (BER) would be minimal.

A wide variety of technologies are found in modern commercially available and custom links. The diode geometry is a first order concern. Receiver diodes for single mode optical detection may have diameters as small as 25 microns, whereas some commercial links do use multimode devices that are hundreds of microns in diameter. Thicknesses may be ~2 or 3 microns for direct bandgap detectors in III-V compounds to ~40 microns for indirect bandgap Si structures. The receiver must be chosen with a response to match the transmitter wavelength which typically is ~850 nM for GaAs based LEDs and lasers and either 1310 or 1550 nM for InGaAs transmitters. At 1310 and 1550 nM wavelengths, the detectors are almost always thin direct bandgap III-V materials, most often InGaAs based. For shorter wavelengths, e.g. the now popular Vertical Cavity Surface Emitting Laser (VCSEL) transmitters at ~ 850 nM, the detector may be either Si with relatively thicker junctions or direct bandgap GaAs. The GaAs solution is usually found in the higher data rate links because the narrower junction results in higher bandwidth due to lower parasitic capacitance.

Though the photodiode must be large enough to capture the optical signal, it obviously should be no larger since the excess junction would result in both higher parasitic capacitance and, more importantly here, increased "target" area for particle strikes. Our analysis indicates better SEE characteristics for III-V direct bandgap detectors since the depletion depth need only be about 2-3 microns for > 80% quantum efficiency. In contrast with indirect bandgap detectors such as Si for 850 nm applications in which depletion depths are about 20 x larger, the thinner structure minimizes both the "target" size for ion strikes as well as the ion pathlength (and deposited charge) when hit.

A detailed treatment of the various receiver circuit implementations and encoding techniques is beyond the scope of this work, but it should be noted that the effective proton induced BER is affected by the receiver circuitry as well as by higher level encoding schemes. The most significant circuit related effect was alluded to in the discussion of figure 2 with respect to the threshold dependence on the link's optical power. This dependence is only found when automatic gain control is implemented to maintain a variable threshold midway between the signal levels representing a zero and one. As a consequence, in links where AGC circuitry is used, the BER cross section depends on the optical power incident on the receiver diode. One example of this is shown in the data of Figure 3 [from 8]. Further discussions of BER circuitry dependence and encoding schemes can be found in [7-11], but we note the need for an error rate prediction technique to be applicable to a range of implementations in the physical layer as well as circuit and protocol levels.

The data of Figure 3 illustrate other important clues to the physical mechanisms underlying the proton induced errors. Note the "proton counting" characteristics at lowest optical powers, where the cross-sections are largest. The family of curves corresponding to various angles of incidence (90 degrees is grazing incidence) converge to nearly the same cross-section which in turn corresponds to the projected physical area of the 75 micron diameter device. At higher optical powers, the curves are well separated, and cross-sections at grazing incidence are much higher than at oblique angles for which the shorter path lengths result in less deposited charge. This is characteristic of receivers with AGC circuitry.

Figure 4 shows the details of the angular dependence of another AGC based link around grazing incidence (0 degrees in this case) [12]. These data are from the Honeywell Ruggedized Link® which operates with 12 channels at 1.062 Gbps per channel with 850 nm VCSEL array transmitters and 850 nm GaAs p-i-n array receivers. Since traditional FOL error cross section plots have shown trends versus data rate, optical power, or effective LET, the pronounced cross section trends around grazing angle incidence may have been overlooked by some. In this linear plot at three different optical powers as measured using 63 MeV protons, the data shows a pronounced enhancement in the cross section around grazing angle incidence. Note that each of these optical powers is well above (at least 10 dB) the receiver sensitivity.

To round out this section on physical mechanisms, we note the recent work of Faccio, et al., which addresses the case of a link optimized at the physical layer to minimize particle induced BER impact [13]. The application is for data transfer at a relative modest rate of 80 Mbps in a particle physics environment dominated by neutrons and protons with energies up to ~100 MeV. Link hardware was selected for operation at 1310 nM using an 80 micron diameter InGaAs p-i-n diode in the receiver. The receiver sensitivity allows operation down to optical power levels of ~ -35 dBm, however AGC circuitry is implemented and optical power budgets are managed to assure operation at above -20 dBm to mitigate charged particle impact on the BER. Faccio and coworkers demonstrate with both experiment and simulation, based on the FLUKA Monte Carlo transport and particle interaction code, that under these conditions the role of direct ionization is

effectively suppressed so that the error rate is dominated by nuclear inelastic recoils for the cases of both protons and neutrons. In this regime, the authors note the absence of the cross section dependence on proton angle of incidence, and they provide simulations based on the FLUKA code to predict the resulting error rate from the expected spectra of protons and neutrons.

For fiber optic links, we have described a rather complex mix of physical layer, circuit level, and protocol level implementations for which the physical interactions may be dominated by either direct ionization or nuclear inelastic interactions in the receiver's photodetector.

2.2 Optocouplers: Optocouplers, because of their COTS orientation, typically use low-cost design approaches that target high yield above minimum performance levels. Optocouplers are hybrid devices, and while some vendors are attuned to the specialized needs of the aerospace community, most are not. Traceability of internal components is not the rule, and as a result device-to-device and lot-to-lot variability in radiation response is common. Receivers are usually not optimized for sensitivity as in FOLs, since LED's with sufficient light output to operate the close proximity link are easily available. Optocoupler receivers are usually based on low cost photodetectors that may be configured either as photodiodes, phototransistors, or photodarlingtons. In all cases, the detected optical signal supplies the base current to a gain stage transistor element, and dual gain stages are often used to achieve sufficient output currents to drive following circuitry (see Figure 1). The simplified receiver architectures do not include the AGC circuitry described for FOL receivers, and consequently the optocoupler drive current is not a factor in determining sensitivity to particle induced transients.

The discovery and characterization of the physical mechanisms governing optocoupler sensitivity has followed a similar path to that of FOL receiver sensitivity, though this is a more recent concern. Since the first paper identifying the mechanisms in 1997 by LaBel, et al. [6], subsequent studies by several authors have further characterized mechanisms and offered suggestions for test needs and rate prediction strategies [2, 14-18]. The initial work identified the sensitivity in high speed (> ~5MHz) devices, and described the role of direct ionization from protons in the coupler's internal receiver photodetector. The error condition results from deposition of charge in the detector that leads to a transient that propagates during the "off" state of the device. Errors can occur when ions initiate transients with sufficient pulse width and voltage amplitude, provided the optocoupler amplifier stage is of sufficient bandwidth to propagate the signal to the optocoupler output. This situation is quite similar to that described previously for p-i-n diodes in FOL receivers [8], however there are key differences.

Rather than use separate p-i-n structures, the optocoupler detector's diode is commonly incorporated monolithically using conventional bipolar processing methods. The importance of this arises from the fact that, unlike the p-i-n diode structure commonly found in FOL receivers, the p-n junction found in bipolar processes does not collect charge primarily via drift from a fully depleted intrinsic region. Instead, in bipolar p-n junctions, diffusion from the field free substrate bulk may be a significant source of both the optically detected signal as well as the particle deposited charge. Characteristics of optocoupler cross-section measurements consistent with charge collection via diffusion were first noted in [6], and this was examined in [14-16] with indications that diffusion lengths approaching 50 μm could be possible. Proper treatment of charge diffusion would therefore be an important aspect of any rate prediction approach.

Figure 5 shows the characteristic response of a high speed optocoupler (HP 6651) plotting the error cross section versus angle of incidence for proton exposure [after 6]. The enhancement around grazing angle is due to direct ionization from protons, and suggests a low charge threshold and LET dependence for the error cross-section. Except for grazing angles, the cross-section is

constant and presumed to be dominated by nuclear elastic and inelastic interaction recoils. In Figure 6 [from 2], Reed et al. dramatically show the role of direct ionization in that the grazing angle enhancement is pronounced at LETs corresponding to 70 MeV protons, but disappears at ~half the LET corresponding to 230 MeV protons.

In reference [14], Johnston and coworkers examined the lower proton energy (higher LET) regime in 6N134 optocouplers from two manufacturers and showed the cross-section increase at grazing angle could be as much as 3 orders of magnitude at a proton energy of 15 MeV. The energy dependence of the angular enhancement has also been reported by Reed, et al., as shown in Figure 7 for the Agilent HPCL5231 high speed optocoupler [18]. Note the striking similarity in this behavior as compared to the Honeywell Ruggedized fiber optic link receiver data of figure 4. This suggests that while there are differences in the details of the physical mechanisms responsible for errors in the two types of devices, there may be enough similarity so that a common approach can be used for rate predictions.

In [17], Johnston et al., investigated the response of the HP 6N134 to heavy ions and showed that in addition to the photodiode, amplifier stage circuitry could be susceptible to ion induced transients, and transients with longer time signatures would result. In the interplanetary galactic cosmic ray (GCR) environment, the response to heavy ions should not be overlooked, but in trapped or solar proton environments, the error rates would be dominated by direct ionization from lower energy protons at grazing incidence.

As a final remark on the topic of mechanisms and optocouplers, we note that in the study by Reed, et al. [18], the authors noticed a significant part-to-part variability in the transient error sensitivity as indicated in Figure 8. Presumably, this follows from the COTS nature of the manufacturing process and part-to-part variability in the gain stages, but this has implications for the confidence interval appropriate for a predicted error rate, as well as the number of parts that should be tested and number of date codes, or buy lots sampled.

For optocouplers, we have described a sensitivity in high speed devices that arises from direct ionization from protons. The degree of enhancement can be a strong function of proton LET. The material system is typically Si, and the diode is implemented in a bipolar process for which charge diffusion play an important role. At oblique angles, the proton induced error rates are dominated by nuclear elastic and inelastic reaction recoils. In GCR dominated environments, the contributions to the gain stages cannot be ignored, and temporal response of the error may vary.

2.3 Other Detectors: Ion induced charge deposition in detector volumes for imaging and related applications is important and closely related to the problem of charge deposition in both FOL and optocoupler detectors. CCDs and hybridized imaging arrays are comprised of large numbers (e.g. millions) of pixels, each of which represents a collection volume with lateral dimension of a few microns to a few tens of microns. Often the sensitivity and associated noise levels are optimized for small signal detection, and again, even lightly ionizing particles can corrupt the collected information.

The material systems used for imaging varies according to the wavelength of the optical signal of interest. Typically, Si is used for visible and near ultraviolet imagers, and InSb, HgCdTe, or specially doped (blocked impurity band) Si detectors are used for infrared applications. Collection of the signal may be entirely through drift in fully depleted technologies, but more often it is a combination of both drift and diffusion from field free regions, as in the case of Si bipolar junction diodes used in optocouplers, as depicted in Figure 9 [19].

Modeling of the physical processes has received considerable attention, and a key reference exists for the case of visible Si CCD based imagers that includes both the drift and diffusion contributions [20]. A parallel treatment exists for infrared HgCdTe based hybrid arrays [21]. In each case, the portion of the model that accounts for the diffused charge is based on a model first described by Kirkpatrick [22]. Specialized transport models to assess the particle environment at the pixel level are needed to fully describe the physical processes [23]. Currently, work is under way to integrate the charge transport and charge collection processes and also include the production and effects of secondary particles [19]. Elements of this approach may prove useful for the more precise treatment of the closely related problems associated with errors in photodetectors for FOLs and optocouplers.

## 3.0 History of Rate Prediction Approaches in Fiber Links and Optocouplers:

3.1 Fiber Optic Link Receivers: Fiber optic link receivers were the first digital microelectronic components reported to have sensitivity to the direct ionizing effects of energetic protons, so no validated models were available for assessing on-orbit rates in this regime. Initial studies examined large area (~$10^{-3}$ $cm^2$) p-i-n diodes fabricated in Si with depletion depths of around 40 microns [5]. Because of the sensitivity of the associated circuits, even very energetic protons with low LET deposited sufficient charge to result in bit errors, regardless of the angle of incidence and trajectory through the p-i-n structure. For this limiting "proton counting" case, the expected on-orbit error rate calculation was reduced to the calculation of the arrival rate of protons behind the shielding of surrounding structures. Comparisons between predicted and observed error rates in low earth orbit aboard the NASA SAMPEX satellite showed excellent agreement [5, 11] and confirmed the sensitivity to protons beyond question, though it should be mentioned that error tolerant Manchester encoding (i.e. with a mid bit transition) schemes resulted in completely successful operation.

Lessons learned [1, 6, 8] from first generation (and highly successful) FOLs indicated the mitigating effects of link operation at higher optical power levels and also hardware advantages inherent with selection of direct bandgap semiconductors used in very thin p-i-n structures. With these advances, the proton counting regime ended. Proton LET and angle of incidence (for reasons other than the diode's projected area) were increasingly important in determining the probability of an event resulting in an error. In [8] the error cross-section data for a FOL was first interpreted in terms of proton direct ionization sensitivity using techniques familiar to more conventional cosmic ray SEU prediction techniques. It was suggested that by examining test data in terms of the "effective" LET using proton LET and pathlength information, the data could be fit using the familiar Weibull distribution. Using this relation, the standard models for orbital error rate calculations embodied in tools like the web-based CRÈME-96 code [24] could be exercised with minor modifications. Following discussions will examine the usefulness and possible problems with applying the CRÈME-96 tool (and Weibull based description of the sensitivity response function) in this regime.

Customarily, we have presented FOL cross section data in a format that plots the error cross section versus "effective" LET at a given data rate and link budget optical power [8]. Irrespective of the data rate and optical power, it has been demonstrated that the data can be conveniently fit using the Weibull relation, and therefore is well suited for rate prediction using the assumptions we are familiar with from CRÈME-96. In figure 10 we reproduce a figure from reference [8] which demonstrated that proton cross section data, using various proton energies and angles of incidence, could be reasonably well described by Weibull distributions of cross section versus effective LET. The distribution best describing the trend varies systematically according to the receiver's incident optical power.

In [8], it was further shown that while the Weibull fits offered unique solutions at a given link optical power level, the trends with data rate at a fixed optical power suggested that the results would scale with data rate. This relation is shown in Figure 11 [after 8] indicating that for a link with AGC receiver circuitry the error cross-section is proportional to data rate across a broad range of particle LETs and link optical power levels. So for a given optical power, the observed proportionality to data rate would allow estimates of link bit error ratios (BERs) at other data rates by a simple scaling relation. The relation between the BER, error cross-section, $\sigma$ [$cm^{-2}$], proton fluence,$\varphi$ [cm-2], and data rate is provided in equation 1.

$$BER = \frac{\#\,errors}{Bits\_Transmitted} = \frac{\sigma \cdot \phi}{Data\_Rate} \tag{1}$$

From this we note that since the trend illustrated in Figure 11 depicts a linear relation between cross-section, $\sigma$, and data rate, the result for this special case is a BER that is independent of data rate for a given orbital environment. In hardware FOL implementations for which this relationship can be verified, this result can be used to substantially limit the needs for test data covering a broad range of data rates. Additional data, shown in Figure 12, on other hardware with AGC implemented (Honeywell Ruggedized Link®), do reveal similar trends over optical power [12]. The trends with data rate are similar, but closer inspection in Figure 13 shows a greater than linear increase, so care should be exercised when relying on scaling relations to predict error rates. Moreover, the approximate proportionality with data rate would be expected only in the case of links with AGC based receivers, and similar trends have not been identified to describe the BER tendency over LET and optical power. Obviously, test data should be acquired at the anticipated application data rate(s) if at all possible.

Other more recent link data offer additional challenges for the applicability of the Weibull-based approach on new data measured on the Hewlett Packard HFBR-53DE transceiver set and on the Honeywell Ruggedized Link® transceiver set [12]. Figure 14 shows interesting results of the HP link with cross-sections measured versus incidence angle for five different optical powers. The top curve, corresponding to minimal optical power, is apparently in saturation (operating in the proton counting mode) and reflects the projected area of the photodiode in the beam. At higher optical powers, the cross-section is lower at all angles, but the relative enhancement at grazing angle becomes more pronounced as the link margin is reduced. In the later case, the trends are very similar to that reported in optocoupler photodetectors.

Unfortunately, due to package penetration issues, testing with higher LET protons and He ions was not possible, so data comparing cross section with effective LET are not shown. Hence, in this case Weibull-based rate prediction based on trends with measured cross-section dependence on effective LET is impossible. As discussed in [12], package penetration issues also limited the ability to gain effective LET information from the Honeywell Ruggedized Link® transceiver set as well as another pair for hardware sets from LaserMate®. We recognize package penetration as an important problem in acquiring the data necessary to characterize error cross sections according to effective LET. In particular, determination of the proper value of the saturated cross-section is in question without the higher LET particles. We see no easy solution to this concern since, unlike optocouplers, the FOL receiver necessarily must have intact packaging in order to acquire the necessary data for error cross sections.

Assuming test data are available and parameters describing a fit to the data using the form of the Weibull distribution can be determined, one recommended approach [8] is to use the CRÈME-96 code to calculate the LET spectrum specific to the environment and shielding. With knowledge of the photodiode geometry, the CRÈME-96 routine can then be used to generate a chord distribution approximating that of the omnidirectional particle environment, and fold the LET distribution in with the Weibull description of the cross section dependence to arrive at an

estimate of the orbital error rate. There are three important issues to mention relative to this process. First, most photodiode geometries are best approximated as right circular cylinders and not as rectangular parallel-pipeds (RPP) as assumed by the CRÈME code. The recommendation is to input lateral dimensions of a square RPP of equal surface area as the photodiode and use the CRÈME code determination of the chord distribution as an approximation. More will be said on this section 5.1.1.

The second concern is for proper treatment of the material system, and this affects both the LET distribution as determined in the CRÈME code and the charge yield in the detector for a given LET. For Si detectors there is no issue, however for many FOL implementations the detector material system is GaAs, InGaAs, or some other compound, and the Weibull distribution should reflect the effective LET for the appropriate material. The original CRÈME code allowed calculation of LET in both Si and GaAs; however the current version (CRÈME-96) does not. Computationally, close approximations could be addressed with transforms to account for the difference in LET and in the bandgap-dependent ionization potential which determines charge yield. However, the mechanics for accomplishing this are not present in the CRÈME-96 routine, and therefore one must either limit the CRÈME based assessment to Si devices, or use the earlier version of the CRÈME routine to treat GaAs based detectors.

The third concern in using CRÈME in this application is based on the code's origins and intended application toward cosmic ray induced SEU in microelectronic devices. Use of the HUP routine in CRÈME-96 to treat the ionizing effects of protons is not its intended use, and the LET regime is orders of magnitude below that of most cosmic rays of concern for SEU. There are outstanding questions about the accuracy of the numerical integration approach in this regime, and more will be said on this in a later section.

The only other technique that has been reported for error rate prediction in FOL detectors was proposed by Faccio, et al. [13] for the case of high energy proton and neutron induced errors in a particle collision experiment environment. In their application of the FLUKA code [25], detailed cross-sections were calculated for various proton energies and arrival angles in an 80 micron diameter two micron thick InGaAs p-i-n photodiode. The calculation involved Monte Carlo transport and interaction mechanisms that account for the ionizing effects of the particles, including straggling, and also the inelastic recoil production and secondary particle ionization. Delta rays were also accounted for. Error criteria were simulated as a function of optical power by estimating a cutoff at half the signal level associated with the charge representing a "1" as suggested in [8]. This follows from the mid-level thresholding for AGC based receivers depicted in Figure 2. By simulating the receiver error cross-section over a range of optical powers, several major features of the measured response were reproduced, but not all. The simulation did distinguish between regimes of lower optical power associated with errors from direct ionization versus higher powers where inelastic recoils dominated. Error rates for the intended application were estimated by customized numerical codes used to fold the error cross section together with the predicted environment. See the reference for a more complete discussion of the approximations, limitations, and successes of this approach, but we note that this appears to be a fundamentally sound method for application to satellite FOL applications, though availability of the customized tools required for this are obviously an issue.

3.2 Optocouplers: The development of rate prediction techniques and flight data comparisons for optocoupler transients is in many ways comparable to developments with FOLs. The suggestion has been made that the Weibull-based techniques and CRÈME-96 tool described for FOLs could be applied to optocoupler transient rate predictions [2]. In some ways, since optocouplers are almost always Si based, the CRÈME approach would seem better suited for this application. Reed, et al., provided a study of the Agilent HCPL-5231 optocoupler transient error characteristics versus effective LET which combined data from protons of various angles and

energies with several heavy ion species to cover almost 4 decades in effective LET [18]. Figure 15 shows the smoothly varying trend described by the data which confirms the role of direct ionization by protons and show characteristics of threshold cross section and saturated cross section that can be described by the Weibull distribution [18]. We note that collection of this data required careful modification of the optocoupler package so that short range particles could strike the diode, and exposure at grazing angles with short range particles remains a problem. Package modification rendered the device nonfunctional as an optocoupler, and line of sight access to the detector diode (including grazing angles) must be attained without affecting the electrical performance of the receiver.

Flight data for the HCPL5231 optocoupler, shown in Figure 16, reveal errors both in and out of the proton belts (South Atlantic Anomaly) [18]. Based on test data and radiation environment in this orbit, and considering an effective 50 μm sensitive volume depth, the authors estimated the SET rates with the CREME96 PUP and HUP routines. Their approach was to linearly combine the proton induced inelastic recoil induced errors with those due to direct ionization. The inelastic contribution was predicted using the CREME96 PUP routine (this assumes the Bendel formalism discussed in section 4), and the direct mechanism prediction used the CREME96 HUP routine in I96 with the assumptions and techniques previously discussed. The estimated upset rate induced by Galactic Cosmic Rays (GCR) is ~0.05/day which is in good agreement with on orbit data (~20 predicted versus ~7 observed). The estimated upset rate induced by trapped protons is 1/day, and we find that the proton direct ionization contribution to this rate is about 70%. This predicts the on orbit rate to within a factor 4. Based on the uncertainties in the prediction method (size of sensitive volume, AP-8 model uncertainties, detailed shield analyses, etc.,) and very significant part to part variation (recall Figure 8), the authors concluded that the prediction is in "very good" agreement with the observed on orbit event rate.

Other approaches have also been recommended to treat optocoupler error rate predictions. In [14] extensive data were acquired on the 6N134 optocoupler that demonstrated the error cross section dependence on angle of incidence and proton energy (LET) for protons. Rate prediction was addressed and rather than advocate an approach based on effective LET, the suggestion was made to empirically determine an effective cross section at a given proton energy by integrating the cross section over all arrival angles and establishing an average cross section for a given proton energy. By measuring the angular dependence over the necessary range of energies, and determining the appropriate "effective" cross section dependence on energy, the cross section data could be combined with proton spectra to arrive at an empirically based effective rate.

This approach may be suited to the problem of rate prediction for an appropriate data set, but we note that the energy and angle dependent error cross section data requirements to support this analysis are extensive. Also, as in the Weibull approximation approach, there are very serious difficulties associated with testing with low energy protons at high grazing incidence angles as a result of particle range issues. Finally, the numerical tools necessary to fold the environment together with the error response function are not "standard" items. Even so, this purely empirical approach does offer the advantage that no knowledge of the material or geometry of the detector diode is required for the analysis. Also, there are no assumptions or explicit treatments specific to charge diffusion in bipolar devices or if indirect versus direct proton interaction mechanisms, though the authors in [14] do concur that the observed trends are consistent with the majority of errors following from direct ionization by protons. More on test issues and comparison with the effective LET based approach will be presented in the following sections.

## 4.0 Standard Rate Prediction Approaches and Their Applicability to This Problem

Section 3 described reported applications at either direct use or modification of existing tools to predict the error rate effects of charged particles, first in FOLs and then optoelectronics. In this

section, we will describe, in more detail, the capabilities and trade-offs involved with use of a more complete set of predictive tools used to assess single event effects in satellite components.

## 4.1 Indirect Mechanism from Proton Induced Nuclear Reactions:

4.1.1 Bendel One and Two Parameter Models: Conventional treatment of proton induced upset in memories and microelectronics deals only with the indirect mechanism, since direct ionization cannot deposit enough energy to cause upset. The details of the semi-empirical formalism for rate prediction described first by Bendel are discussed in [26 and references therein]. For old devices with large dimensions, determination of the proton cross-section at a single energy was considered sufficient to permit a fit using the Bendel one-parameter function, which is given by:

$$s = (24/A)^{14}[1-\exp(-0.18Y^{0.5})]^4 \quad (2)$$

with $Y=(18/A)^{0.5}(E-A)$, and where proton energy, E and the fitting parameter, A are in MeV. The cross-section is given in terms of upsets per proton per $cm^2$ per bit. However, the data obtained for more modern microelectronic devices do not fit the 1-parameter function very well, and often fits are now done with the Bendel 2-parameter equation. The two-parameter Bendel function [26 and references therein] is given by:

$$s = S\,[1-\exp(-0.18Y^{0.5})]^4 \quad (3)$$

where S is the proton limiting cross-section and Y is the same as in the 1-parameter Bendel equation. Of course the 2-parameter option requires that data be measured at multiple energies.

Sections 2 and 3 described data on both FOL receivers and optocouplers that in some cases appeared to be dominated by errors with characteristics of this indirect mechanism. With optocouplers, as illustrated in Figures 5-8, the cross section is independent of angle, except for near grazing incidence. We interpret this as an indication of the indirect mechanism, and would expect the Bendel-based prediction to be an appropriate approach in this regime. At present, there are no data sets to test the applicability of the one parameter versus two parameter Bendel approaches. For fiber based links, reference [13] illustrates that at high optical powers the error rate can be dominated by inelastic collisions, and again we would advocate the use of the Bendel formalism for cases where it can be shown that direct ionization is unimportant.

4.1.2 Weibull Description of Proton Indirect Ionization: In some cases, event the 2 parameter Bendel model does not allow adequate fitting of proton energy dependent cross section data. The Weibull fit with functional form indicated in equation (4) has been recommended as an alternative to describe the energy dependence of indirect upset mechanisms from protons [26a]

$$F(x) = A\,(1- \exp\{-[(x-x_0)/W]^s\}) \quad (4)$$

where x is the effective LET in MeV-$cm^2$ /milligram, F(x) is the SEE cross-section in square-microns/bit, A is the limiting or saturated cross-section, $x_0$ is the onset parameter such that $F(x) = 0$ for $x < x_0$, W is the width parameter, and s is a dimensionless exponent often referred to as the shape parameter.

The Weibull distribution is often used to describe heavy-ion direct-ionization induced SEE cross-sections. However, it has been shown that in some devices, a Weibull function also gives a better empirical description of the proton-induced SEE cross-section. The CRÈME-96 code [24] does

offer the options of either 1 or 2-parameter Bendel fits or Weibull fits to proton data. Obviously, testing at several proton energies is required for reasonable accuracy.

4.1.3 CUPID, MCNP-x, GIANT-4, FLUKA and other Transport and Monte Carlo Interaction Codes: The development of specialized nuclear physics based codes to calculate energy deposition for microdosimetry and single event effects goes back to the early 1980's when proton induced reaction SEE first became a concern. A thorough discussion is contained in [26 and references therein]. McNulty and others have developed the CUPID code specifically to address the SEU problem and include nuclear elastic and inelastic scattering for most of the possible interactions for Si and GaAs. The CUPID code has been validated against data on a broad range of devices. In principle, it could be a valuable tool for assessing error rates in FOL and optocoupler detectors, but the code is not widely available, and the interface requires considerable expertise. Also, the capabilities to generate and input orbital spectra are limited, and treatment of the material and device physics important to charge collection in bipolar diffused and p-i-n photodiodes will require more work.

MCNP-x, GIANT-4, FLUKA and other transport and Monte Carlo interaction codes have been developed primarily by the nuclear particle physics community. Extensive detail is incorporated to provide a Monte Carlo description of the physical interactions taking into account the most recent and complete compilations of nuclear interaction cross section data. FLUKA has already been applied to the problem of proton and neutron error rate prediction in fiber optic link detectors in an accelerator application as described in Section 3 and in [13]. MCNP-2 is being used to evaluate the secondary particle production by proton interactions in satellite structural elements for the NASA Next Generation Space Telescope [19]. And, GIANT-4 has been given considerable attention by the European Space Agency to provide additional capabilities if interest to the satellite community [27]. The enhancements to GIANT-4 include a generalized source particle module for defining the radiation environment with ample flexibility to describe orbital omnidirectional radiation spectra, sectored shielding and transport calculations, production and decay of radioactive nuclei and tracking of decay chains, lower energy cutoffs for secondary particle and photon production, and a user friendly CAD interface. Reference [27] provides further detail, and in many ways this toolkit seems well suited, but incorporation of the device physics of charge production in materials and geometries important to the detector problems may require additional work. Also, there is the issue of availability and level of expertise required to operate the code.

4.2 Direct Mechanisms; CRÈME-96: The CRÈME and CRÈME-96 codes have been the most widely used routines for calculation of SEU in microelectronics due to the GCR environment. CRÈME-96 is the latest in a series of tools which have been developed to be user friendly tools for satellite design engineers and radiation effects specialists to assess the SEU rate based on test data and some knowledge of the device. Details of the code and comparisons with other available tools are found in [26 and references therein]. Another popular package, the Space Environment Information System (SPENVIS) [28] also relies on the CRÈME tool for galactic cosmic ray and solar particle environment definitions. The following summary of the CRÈME code is found, along with additional related information, in the SPENVIS website at [29], and the reference to "(Pickel and Blandford, 1980)" appears in this document as [30].

> "The minimum charge required to produce an SEU is called the critical charge. This burst of charge can come from a segment of the ionization trail left by the passage of an intensely ionizing particle. It is assumed that each critical node is surrounded by a sensitive volume (ionization as a rectangular parallellopiped) and that the charge deposited in this volume is

collected (Pickel and Blandford, 1980). The dimensions of the sensitive volume are related to those of the critical node. The sensitive volume is not, however, just the dimensions of this feature. Charge is also collected by diffusion from the silicon surrounding the node. The efficiency of charge collection from beyond the node falls off with distance. Pickel and Blandford (1980) discuss how the critical charge and the dimensions of the sensitive volume are found. In general, experimental measurements of the operational SEU cross section for the device, as well as design data supplied by the manufacturer, are required. It is often necessary to interpret these data using detailed circuit modeling software before the device SEU parameters can be determined.

The simple model described above predicts that when the critical charge has been collected, an SEU will occur. The amount of charge collected depends linearly on the LET of the ionizing particle and the length of its path within the sensitive volume. There is, however, another effect that extends the size of the sensitive volume. The intense trail of ionization left by the charged particle alters the electric field pattern in the neighbourhood of the feature. The field forms a funnel along the particle track and this enhances the efficiency with which charge is collected. This funnel effect can be partly accounted for in the simple model discussed above if the dimensions of the sensitive volume are experimentally determined.

The method for estimating soft upset rates due to the direct ionization by particles originating outside the spacecraft is described by Adams (1983). The upset rate $N_e$ (in $bit^{-1}$ $s^{-1}$) is given by:

$$N_e = 22.5\,\pi A\,Q_{crit} \int_{22.5Q_{crit}}^{L_{max}} \frac{D[p(L)]\,F(L)}{L^2}\,dL\,, \qquad [(5)]$$

where $A$ is the surface area of the sensitive volume in $m^2$, $Q_{crit}$ is the minimum charge in picoCoulomb required to produce an upset, $L_{max}$=1.05x10$^5$ MeV $cm^2g^{-1}$ is the highest LET any stopping ion can deliver, $P_{max}$ is the largest diameter of the sensitive volume in g $cm^{-2}$, $L$ is the LET in $cm^2$ $g^{-1}$, $F(L)$ is the integral LET spectrum in $m^{-2}s^{-1}sr^{-1}$, and $D[p(L)]$ is the differential pathlength distribution in the sensitive volume of each memory cell in $cm^2g^{-1}$, where $p(L)$=22.5 $Q_{max}/L$ is the pathlength over which an ion of LET $L$ will produce a charge $Q_{max}$. The constant 22.5 is the conversion from pC to MeV, assuming 3.6 eV per hole-electron pair.

The equation for $N_e$ contains the implicit assumption that the LET of each ion is essentially constant over the dimensions of the critical volume. Of course, this is not true for stopping ions very near the end of their range. The equation assumes that the maximum LET of the stopping ion applies over its entire pathlength in the sensitive volume. This assumption can result in calculated energy depositions that exceed the residual energy of the ion. The problem is especially acute for large sensitive volume dimensions and threshold LET values just below the maximum LET of an ion that is much more abundant than all heavier ions. Fortunately, this circumstance rarely arises. The equation for $N_e$ is accurate if the flux of stopping ions is small compared to fast ions having the same LET. Care should be taken in the use of this formula when the threshold LET is just below the edge of a “cliff” in the integral LET spectrum.

The equation above assumes one continuously sensitive critical node per bit. In general, there may be several critical nodes per bit, each with its own sensitive volume dimensions and critical charge. In addition, these nodes may only be sensitive part of the time, making it

necessary to calculate partial upset rates for each node and then combine the results, weighted by the fractional lifetime of each node. "

Aspects of the CRÈME-96 based calculation approach are treated in Sections 2 and 3, and that discussion presumes that an empirical description of the error cross section with LET as described by the Weibull distribution could be used as the basis for the rate prediction. The discussion in the preceding paragraphs do not discuss this, but describe an alternative available using the CRÈME or CRÈME-96 codes based on knowledge of the critical charge and critical volumes. Either or both techniques may be applicable to aspects of the FOL and optocoupler rate prediction problems. The tradeoff has two important aspects. In both cases, the knowledge of the diode material (Si) and geometry are important. For the critical charge approach, estimation of possible alternate charge collection (possible funneling and diffusion in the bipolar case for optocouplers) may be important. The Weibull based calculation does not require explicit knowledge of the critical charge, and it is more sensitive to charge collection and circuit related issues which can affect the shape of the cross section versus LET curve, and would therefore be captured as part of the input data set. Because of this, we consider that the Weibull description could offer better fidelity, but recognize the difficulties in obtaining the necessary range of LETs because of package penetration issues with low energy protons and heavier ions. Unfortunately, there are no complete data sets at this time which would allow a comparison between he two approaches and with flight data.

## 4.3 Combined Mechanisms:

4.3.1 NOVICE: The NOVICE code is a commercially available expert code available from Experimental and Mathematical Physics Consultants (EMP) [31]. The code either generates or accepts user defined inputs from the standard environmental models or from modified input files from Monte Carlo interaction codes such as MCNP-x, GIANT-4 or others discussed in Section 4.1 with capabilities of providing Monte Carlo transport and energy deposition calculations of the input environment, including the effects of secondary particles and delta rays (electrons). The code can be used to accept CAD level drawings of satellite structures for detailed assessments of the particles reaching a user specified location. There is considerable flexibility in the ability to define target geometries to simulate the structures found in detectors of various types, including photodiodes found in FOLs and optocouplers. According to the information found in [31], the inputs and outputs are described as follows:

"Input Description: Geometry's, spectrum, detector locations, materials properties

Output Format: Graphical output of differential and integral spectra, response functions, neutron and gamma ray cross sections and LET, electron range and stopping powers, and heavy ion range and stopping powers, dose vs. thickness, pulse heights, photon attenuation, and particle transport."

The pulse height output mode is of particular interest to the FOL and optocoupler detector problems, and one relevant detector application is discussed in [19]. Another important difference between NOVICE and CRÈME deals with the fact that NOVICE tracks the LET as it changes when traversing the structure and CRÈME assumes that the LET incident at the surface is constant throughout the sensitive volume. NOVICE is also fully capable of the full range of materials and geometries of interest to this problem, and it also treats nuclear elastic and inelastic interactions and subsequent energy deposition. Additional information on NOVICE can be found at http://see.msfc.nasa.gov/see/ire/model_novice.html [31].

4.3.2 JPL Empirical Approach: This strategy is also discussed in Section 3.2 and in reference [14] in the context of rate prediction for optocouplers, though it is in general akin to the Effective Flux Method described by Binder [32] for the general problem of SEU in microelectronics. Binders method has been adapted into a code by Scott [33], and adopted for rate calculations for the International Space Station. Functional descriptions of angle and LET dependences are combined with the environment description in terms of effective LET, and rate estimation follows from integrating the environment's LET function with the response function. This approach does not require the determination of pathlength as part of the rate calculation, but it does require that extensive data be gathered over the LET range of interest and over the range of particle trajectories.

This basically empirical approach may offer advantages where details of the device material or structure are unobtainable, but the test data requirements are significant and ion penetration at the higher LETs is a problem. We include this under the treatment of "combined mechanisms" since there are no *a priori* assumptions about interaction mechanisms. For the case of rate prediction in optocouplers discussed in [14], where there may be a combination of direct and indirect mechanisms with varying roles of charge collection by drift and diffusion, the LET and angular dependencies need not be explicitly since their response is reflected in the measured cross section data.

4.3.3 Piecewise Linear Combination of Direct and Indirect Mechanisms: As the section title implies, this approach might offer advantages in regimes where the aggregate error rate will have significant contributions from both indirect and direct ionization. Since a tool such as CRÈME does not have the capability to assess the indirect component and the Bendel formalism is not appropriate for the direct mechanism, the solution is to parse the measured cross section data into their respective regimes, select an appropriate calculational approach for each, and then sum the two results. This was essentially done in reference [13], though the FLUKA code was used to treat each case separately, and in [14] the authors provided a comparison between their observations using the combined mechanism rate versus assuming only indirect mechanisms.

## 5.0 Case Studies and Tradeoffs of Rate Prediction Approaches:

### 5.1 Comparison Results for CRÈME-96 and NOVICE:

As part of this study we have undertaken a series of calculations to assess the suitability of the CRÈME-96 and NOVICE calculations to evaluate the geometry and charge deposition issues in diode materials and geometries relevant to FOL and optocoupler receivers. For the case of direct ionization we consider that the NOVICE code has the appropriate level of detail to accurately evaluate both the geometric concerns and the particle energy deposition physics for the various materials of interest. So in a sense, this comparative study looks at the ability of the CRÈME-96 code to operate on very low LET protons (outside its intended regime) and replicate the "true" results as determined by NOVICE.

5.1.1 Geometric Issues of IRCC versus IRPP Chord Length Estimations: This comparison looks at the specific issue of the determination of pathlength through the diode structure, and this is one step in assessing charge deposition. As discussed in Section 2.1, it was proposed in [8] that the rigorous treatment of chord length distribution for the Integral Right Circular Cylinder (IRCC) may not be necessary, and the existing tools in (CRÈME-96) to generate the Integral Rectangular Parallelepiped (IRPP) chord distribution could be adequate substitutes.

The suggestion is that, for thin planar structures with high aspect ratios, the chord distribution for the IRCC would not differ significantly from that of an IRPP of equal surface area. Specifically, this was suggested for direct bandgap materials such as InGaAs for FOL application which have a 2 to 3 micron depletion depth and at least a 25 micron diameter, so the aspect ratio would be greater than 10:1. The same question is appropriate though, for indirect bandgap detectors for FOLs and optocouplers for which the effective depth might be 50 microns and the diameter may be only twice that.

To cover the range of geometries and aspect ratios of interest, the chord length calculations were carried out according to the matrix of Table 1 where $d_x$ indicates right circular cylinder diameter and $h_y$ indicates cylinder height. Corresponding rectangular parallelepipeds were constructed to have equal height and square surface area with lateral dimensions to match the surface area of the cylinder. The two geometries are depicted in Figure 17. Since it is not possible to extract the chord distribution as output from the CRÈME or CRÈME-96 codes, the comparison is based only on calculations using NOVICE. Hence, the fidelity between the IRPP treatment in NOVICE and CRÈME is not explicitly determined in this comparison.

Table 1: Matrix of geometries for IRCC vs. IRPP Comparison

| $d_x$ | (μm) | $h_y$ | (μm) |
|---|---|---|---|
| $d_1$ | 25 | $h_1$ | 2 |
| $d_2$ | 75 | $h_2$ | 25 |
| $d_3$ | 200 | $h_3$ | 50 |
| $d_4$ | 400 | | |

Figure 18 shows IRCC versus IRPP calculation results for the case of 25 micron diameter cylinders with thicknesses of 2, 25, and 50 microns. Corresponding aspect ratios are 12.5, 1, and 0.5. As suggested in [8], for the thin planar structure, the agreement between IRCC and IRPP results is excellent, but for low aspect ratios there is significant deviation. For both the 25 and 50 micron thicknesses, the approximation of IRCC by IRPP geometries would lead to overestimation of the longer chords, and corresponding overestimation of deposited charge. The errors appear to be on the order of ~20% or less, and this is probably acceptable, especially since it would be a more conservative prediction.

Comparisons of Figures 18, 19, 20, and 21 indicate the increasingly improving agreement of the chords calculated for the RCC and RPP as the diameter of the diode increases and the aspect ratio grows. Figure 18 shows that for an aspect ratio of 12.5 the results are indistinguishable and errors appear to be only a few percent for aspect ratios of 3 or greater.

We recognize that there is an approximately linear relation between pathlength and charge deposited (exactly linear for constant LET), and that the error cross section dependence on LET is nonlinear. Therefore a 20% error in pathlength may not map into an equal error in the predicted error rate. Even so, the comparisons made here would error on the side of a higher rate prediction if RPP geometries are used, and that more conservative shift does not seem significant for aspect ratios of 3 or greater. We consider that this covers most of the cases of interest, and the chord approximation using RPP geometry, such as that used in the CRÈME codes, should be adequate.

5.1.2 Charge Deposition Comparison for Specific Environments: Having addressed the issue of chord length distributions, our next step is to exercise the CRÈME-96 and NOVICE codes under the same test case conditions and compare the rate prediction results. The first series

of calculations, shown as Figures 22, 23, 24, and 25 further resolve uncertainties associated with chord distributions. The calculation results shown in these figures are for the integral event rate for the matrix of geometries of Table 1.

Rates have been calculated using NOVICE for each of the diode diameters and thicknesses for the test environment of the Solar Particle Event Worst Week Case as calculated in the CRÈME-96 code. This environment has been selected as a typical test case, and does not represent a worst case, and the comparison results would be expected to depend somewhat on the details of the environment. Comparisons within a figure show the trends with diode thickness for a given diameter, and comparison between figures shows how the rates increase with increasing diameter. This set of charts is for Si only. Note that the integral rate is approximately flat for events up to ~ 10 keV, and the intercept represents the "proton counting" regime. Figure 22, corresponding to the 25 micron diameter, shows the most dramatic differences in terms of diode thickness, and these differences are pronounced even at the intercept.

Comparison of rates for the 4 diameters indicates about a 2 orders of magnitude increase in the 400 micron diameter case relative to the 25 micron case at the limiting condition of "proton counting as expected based on area differences. The differences are more dramatic at the high energy deposition (~1 MeV) limit and can exceed five orders of magnitude for a given thickness.

Only very slight differences between the IRPP and IRCC treatments are noted, and these are only in the high energy deposition regime where the longer, but low probability, path lengths across the RPP are possible. Even for the case of 25 micron diameter, and especially for higher aspect ratios shown in Figures 23, 24, and 25, the agreement between IRCC and IRPP treatment is very good.

Figure 26 compares the results of NOVICE and CRÈME-96 calculations of 75 micron right circular cylinders in Si for thicknesses of 2 and 50 microns. The results show a surprising lack of agreement, especially for the thicker dimension, and the CRÈME results do seem suspect in some regards. For example, the indication from CRÈME is that for the 50 micron thickness, the vast majority of interactions deposit less than 100 eV. The upturn below ~ 300 eV seems nonphysical, though the exact reason for the discrepancy is not obvious. In the low energy regime, the comparison for the 2 micron thickness shows better agreement. At higher energy points, the CRÈME and NOVICE results diverge for both thicknesses, with NOVICE consistently yielding higher rates. One possible explanation for this is that NOVICE does track the changing energy and LET as the proton traverses the volume of interest and CRÈME assumes the incident LET remains constant throughout the volume. This approximation in CRÈME would lead to underestimation of the rates for high energy deposition events, but whether this could account for the ~2 order of magnitude discrepancy is not known.

Table 2 compares the CRÈME-96 versus NOVICE integral rates for > 36 eV energy deposition for 12 combinations of RCC diameter and thickness. Note that this is the lowest energy point considered in Figure 26 and corresponds to the "proton counting" regime. The comparison shows good agreement for thin geometries, but very poor agreement for both the 25 and 50 micron thicknesses for all 4 diameters. Given the apparent anomalous trend seen Figure 26, the CRÈME results appear suspect for anything greater than 2 micron thickness. The next series of charts in Figures 26, 27, 28, and 29 shows the same series of comparisons for GaAs, again based on calculations in NOVICE.

Table 2. Comparison of integral rates for the 12 RCC geometries for CRÈME-96 and NOVICE.

| d | h | Si (CREME) | Si (NOVICE) | GaAs (NOVICE) |
|---|---|---|---|---|
| (mm) | (mm) | Integral Rate > 36 eV (events/s) | | |
| 25 | 2 | 0.03 | 0.03 | 0.03 |
| 25 | 25 | 0.31 | 0.08 | 0.08 |
| 25 | 50 | 0.49 | 0.13 | 0.13 |
| 75 | 2 | 0.27 | 0.24 | 0.24 |
| 75 | 25 | 1.43 | 0.38 | 0.38 |
| 75 | 50 | 4.79 | 0.53 | 0.53 |
| 200 | 2 | 1.85 | 1.64 | 1.64 |
| 200 | 25 | 5.09 | 2.01 | 2.01 |
| 200 | 50 | 14.80 | 2.42 | 2.42 |
| 400 | 2 | 7.32 | 6.50 | 6.50 |
| 400 | 25 | 13.80 | 7.25 | 7.25 |
| 400 | 50 | 33.70 | 8.05 | 8.05 |

## 5.2 Material Issues with Existing Calculation Tools:

5.2.1 NOVICE comparison of Si and GaAs: The NOVICE tool has been exercised to calculate energy deposition in GaAs structures for the same set of RCC geometries shown for Si in Figures 22, 23, 24, and 25. The corresponding results for GaAs appear in Figures 27, 28, 29, and 30. Note the similarity in trends, with a bias toward increased rates for higher energy deposition events in GaAs. This is due in part to the greater density of GaAs. For the low energy deposition case (proton counting), the GaAs results are identical to Si. This is expected, and is also indicated in Table 2 which compares the two NOVICE calculations.

The compiled results of calculations for Si and GaAs can be useful for comparative trades. For example, if an 850 nm wavelength FOL receiver were being designed for flight, the information provided here could assess relative expect performance of a GaAs p-i-n structure versus a Si p-i-n structure for a given sensitivity and diode diameter.

5.2.2 Transforms Based on LET and Material Density and Bandgap: Thus far, the NOVICE and CRÈME calculation results have been expressed in terms of energy deposition. Receiver sensitivity would more typically be evaluated in terms of signal level, and both can be interpreted in terms of charge representing either a bit or a particle event.

Ideally, a rate prediction tool would allow definition of both material composition and charge yield for a given amount of deposited energy. In case this is not available, the following relations may be helpful. First, the relations between energy deposited, E, in MeV, and charge yield, C, in picoCoulomb, is given by the following conversion factors. For Si, GaAs, and $In_{.53}Ga_{.47}As$, multiply the energy deposited in MeV by factors of 0.445, 0.383, and 0.592 respectively to obtain charge in pC. These factors incorporate the bandgap dependent ionization potential.

Also, the proton LET energy dependence in InGaAs is essentially the same as that of GaAs. Based on calculations for GaAs and for $In_{.53}Ga_{.47}As$ using TRIM, we note that the physical densities of the two materials differ by only 6% and the LET (in energy per length) agree to within 3% for proton energies up to 150 MeV. When using GaAs to simulate InGaAs; however, it is important to recognize the lower ionization potential of 2.7 eV per ion pair for the narrower bandgap InGaAs alloy versus 4.21 eV per ion pair in GaAs [8]. This is rather easily handled by a systematic 56% increase in the charge deposition results of the CREME calculation for GaAs, e.g. the results describing the number of particle events exceeding 10.0 pC in GaAs also applies for the number exceeding 15.6 pC in the same geometry with InGaAs.

6.0 Summary and Recommendations: In this section, we combine the issues of physical mechanisms with current technology trends, test needs, and flight data to arrive at recommendations for a rate prediction approach. This is assessed first for FOLs and then for optocouplers. After looking at leverage and synergy with rate prediction tools for other sensors, we then consider the prospects for a common prediction approach and tool for FOLs and optocouplers.

6.1 Status and Recommendations for Fiber Data Links: Sections 2.1 and 3.1 described the physical mechanisms of proton interactions with FOL receivers and the published suggested approaches for error rate prediction. In this section, we will provide a closer examination of the current state of our ability to take a generalized approach to FOL testing and error rate prediction. We will begin by examining currently available technology and development trends, then examine test needs and fidelity of prediction attempts with flight data, and conclude with recommendations for prediction approaches with additional comments on uncertainty. To some extent, the accuracy required in the prediction by a given application will dictate the level of effort in testing and rate prediction. We will attempt to indicate where shortcuts to bounding calculations may be appropriate, as well as methods required where more precision is needed.

6.1.1 FOL Technology Trends and Tool Requirements: Choices of potential flight hardware are growing rapidly due to the commercial interests in high performance networking hardware. For many NASA applications, there will likely be well suited existing COTS solutions to FOL requirements. Also, as with the Small Explorer Data System AS-1773 FOL development [5], there will also likely be future needs to develop customized solutions, but almost certainly this will be done with leverage on the COTS component base.

The tools being developed today will also find related applications beyond FOLs in fiber based gyroscopes, fiber sensors, free space optical interconnects and links, analog fiber links, and others. More on the directions and challenges of inserting new photonic technologies into flight projects can be found in [34]. With focus on the receiver function and in particular on the photodiode, the next few years should continue see applications of the same 3 basic wavelength choices of 850, 1310, and 1550 nanometers. Additionally, insertion of quantum well lasers for 980 nm operation may be considered for flight. Higher speed links may find advantages in MSM or Schottky structures, and avalanche photodiodes (APDs) also represent a possible category that has been shown to be very sensitive to protons [35]. Even so, we expect that most of the needs for the next few years will be met with traditional p-i-n diode based receivers in Si, GaAs, or InGaAs. With regard to tool development, the ability to embrace all potential hardware choices seems more a desire than a requirement, and we recommend the focus on p-i-n structures reflecting the range of diameters indicated in Table 1 and with ~40 to 50 micron thickness for Si and ~2 to 3 micron thickness for GaAs and InGaAs.

Today's trends toward brighter and more efficient sources as well as highly parallel architectures will assure that FOL hardware choices that operate with minimal sensitivity to proton direct ionization will be available for many applications, but operation at receiver maximum sensitivity will also remain a possibility, provided error impact is unimportant or error tolerant solutions are implemented. Consequently, we consider it a requirement that the tool cover the full range from proton counting with maximum sensitivity to direct ionization to more tolerant high optical power links where indirect mechanisms are more important.

6.1.2 Test Needs and Recommendations for FOL Error Rate Prediction: Requirements for testing should reflect the amount of confidence needed in the error rate prediction. Back of the envelop estimates and worst case upper bounds can be made even without testing, provided there is adequate knowledge of the materials and circuitry. But in most cases, we see no substitute to *in-situ* testing with link operation in data transfer mode with some fidelity to the intended application. This is usually accomplished with a bit error rate test set as shown in Figure 31 (after [8]). Higher precision estimates will place more demands on the level of detail required in the test effort, and this may be further complicated by packaging issues.

We will examine three cases that represent realistic scenarios and then discuss the associated test requirements to support rate prediction for each. A summary of testing requirements is provided in Table 3. First, consider the worst case upper bound. For this purpose, and with caution, the CRÈME-96 code can be used, provided knowledge of the diode geometry is available. Note that the limitation that CRÈME-96 treats only Si is not an issue here, since results are material independent in the proton counting regime. This routine is readily available on either the CRÈME or SPENVIS websites [24, 29], and incorporates the standard models for trapped, solar, and galactic protons and other ions. The worst case upper bound rate can be determined by assuming a low critical charge (on the order of 5E-4 pC) and providing a description of RPP geometry that matches the thickness of the diode structure and has square lateral dimensions so that it matches the surface area of the actual diode. As shown in section 5.1.1, this approximation to the actual diode shape is very good. If the diode is thin (2 or 3 microns), then there is no issue, but care should be taken for diodes of greater thickness if the CRÈME-96 routine is used for the reasons described in Section 5.1.2. For example, if the diode were Si, then a 40 or 50 micron thickness would be appropriate and recalling the trends of Figure 26, it is important to select a critical charge higher than the anomalous upturn seen at the very low end of the curve (around 5E-4 pC). We recommend a series of calculations starting with very low critical charge and choice a rate corresponding to the flat part of the curve.

If the worst case upper bound seems unacceptable and unrealistically conservative, the next step would be a rate estimate based on estimation of critical charge. Critical charge can usually be estimated with some knowledge of the receiver circuit. For fixed threshold receivers, the critical charge is straightforward. For receivers with automatic gain control, critical charge can be approximated according to the charge associated with the average optical power level when incident on the receiver for one bit period, as suggested in [8, 13]. The minimum expected optical power should be considered for this purpose, including end of life effects, to provide the most conservative estimate.

Testing may also allow estimation of critical charge, but this is a bit more complicated in the case of proton direct ionization because of the existence of the indirect mechanism. Critical charge may be estimated based on the LET, diode material, and pathlength at which the cross section shows significant departure from the angular independent response associated with the indirect mechanism. If testing is done to assess this, it should be done with the lowest anticipated incident optical power, and at the data rate or rates important to the application. If the optical power

regime is low, then it may not be possible to identify a departure from the indirect mechanism, and this approach to estimate critical would not work. The receiver circuit analysis described in the previous paragraph should offer guidance as to whether testing might be expected to be a viable approach to assessing critical charge.

Once critical charge is determined, rate prediction based on RPP assumptions seems appropriate, but because of the problems with the CRÈME-96 model described in section 5, we caution against its use. (Recall that the program does not treat materials other than Si.) Although transforms can be used to interpret CRÈME-96 results for Si in terms of response in GaAs of InGaAs, these approaches are cumbersome and not exact. Also, with thicker structures (i.e., Si detectors), there are issues with the CRÈME based predictions for proton direct ionization effects at both high and at low critical charge. At low critical charge, the error results in overestimation of the rate, but at higher critical charges CRÈME could underestimate the rates from direct ionization by as much as two orders of magnitude.

FLUKA has been demonstrated for this purpose [13], and GIANT-4 and NOVICE should also be well suited. Unfortunately, these are expert codes, and no widely available tool that is well suited for this problem currently exists. One advantage in using the more capable codes is that they can be exercised to treat both the direct and indirect mechanisms. If the critical charge is high, then rate estimation should be approached as a sum of the direct and indirect contributions as discussed in Section 4.3.2.

For the highest accuracy in rate prediction, we advocate the combination of thorough testing with the use of a prediction tool to fold the detailed cross section information together with the environment. The empirical approach described in [14] would be well suited for this, but the Weibull approximation to the data also seems appropriate and should be less data intensive in the high LET regime.

Collection of the data to determine the appropriate response function or Weibull distribution is a bit more complicated. Some attention should be given to the optical power(s) to assure that worst case and end on life conditions are represented by the lowest anticipated power level, and testing at typical levels may also be desired. Testing at various incidence angles with a high density of points around grazing incidence would also be necessary. This allows identification of the indirect mechanism role, if it dominates at lower LETs, and it also allows collection of multiple points to map out trends with effective LET using IRPP assumptions [8]. If the link is intended for broadband use, testing over data rate should be done. The trends discussed in Section 3.1 may be used as guidance, but they are no substitute for test data in high precision predictions are needed, and test data at the anticipated operating rate is recommended. Often, especially for COTS transceivers, it may not be possible to modify the DUT package to gain access for high LET protons and heavy ions. This represents a significant challenge to both the empirical method and the Weibull prediction. In the absence of the ability to test with low energy protons and heavy ions, the saturated cross section may be estimated by the physical area of the diode, but where possible, various proton energies should be used to identify the trends of the indirect mechanism for high proton energies and to map out trends with effective LET at low energies. Because of test issues that have been identified with optocouplers (Section 6.2.2) we recommend tuned rather than degraded beams, especially when measuring at near grazing incidence. Finally, we recommend protocol level testing (e.g., link operation with packet traffic and error correction according to the application) for highest fidelity to the intended application, especially if there is a need to assess error mitigation functions.

Table 3: Test and Predictive Model Input Requirements for FOLs

| | Worst Case Upper Bound | Critical Charge Estimate | Best Estimate |
|---|---|---|---|
| Diode Geometry | x | x | x |
| Diode Material | | x | x |
| Critical Charge | | x | |
| Measured σ vs Optical Power | | | x |
| Measured σ vs Incidence Angle | | | x |
| Measured σ vs Data Rate | | | x |
| Measured σ vs Proton Energy | | | x |
| Measured σ vs Effective LET | | | x |
| Protocol Level Testing | | | x |
| DUT to DUT Variation | | | x |
| Estimated Prediction Error | 10x to 100x | ~5x to 10x | ~2x to 5x |

Combination of the Weibull-based environment description with the environment with IRPP assumptions does appear to be a sound approach, but again we caution against the use of the CRÈME code. The discrepancies in the CRÈME results were found with NOVICE through comparisons based on critical charge and not Weibull cross section descriptions, but we suspect that the same numerical integration issues and assumptions about surface LET will lead to errors in the CRÈME results irrespective of the data input mode. However, the NOVICE code is fully capable of accepting descriptions of error cross section as Weibull parameters, raw data, or other user defined formats [36]. In addition, NOVICE can either generate or accept as input files all of the necessary descriptions of the environments and provide detailed transport calculations to track direct ionization energy deposition in the user defined diode as well as energy deposition from nuclear elastic and inelastic recoil products.

6.1.3 Comparisons with Flight Data: To date, there is a fairly limited amount of flight data available on FOLs, and all examples are some version of the AS-1773 telemetry and control bus or its predecessor the MIL-STD-1773 bus described in [11]. Reference 11 describes flight data and predictions, and Figure 32 form that reference shows the good agreement. In this case, the predictions were made based on a geometric cross section and sensitivity in the proton counting regime. Subsequent predictions with the CRÈME code also showed good agreement, but with the fortuitous evaluation for events over ~6000 electrons, which is where the NOVICE and CRÈME results happen to agree.

In addition to the Small Explorer Data System (SEDS) hardware on SAMPEX, other versions of the AS-1773 have flown on the Photonics Space Experiment (PSE) [37] and on the Microelectronics and Photonics Space Experiment (MPTB) [38, 39]. In those cases, proton dosimetry information of sufficient detail was not readily available to offer opportunities for comparisons, and orbit details were not described well enough to attempt predictions. In the case of PSE, there were comparisons of nominal and worst case link optical power budgets and as expected the lower power showed increased error rates by about a factor of 2. BER rates of ~1 to 4 E-9 were measured, and there were indications that some errors were due to energetic electrons.

The NASA Dual Rate 1773 experiment was characteristically different that the previous to flight hardware sets in that in incorporated a 1300 nm optical layer implemented with direct bandgap

InGaAs photodiodes, and additional circuit based error mitigation approaches were also incorporated [39 and references therein]. Two versions of the link were flown, and error rates on both were low at 8.3 E-13 and 7.7 E-10 for Modes 1 and 2 respectively. The higher error rate in Mode 2 appears to be related to modal reflections in connector bulkheads rather than radiation. We note that these results are consistent with expectations of improvements at 1300 nm and with the transceiver circuit SEE hardening efforts, but detailed comparisons between observations and expectations have not been reported.

In summary, there is simply not yet sufficient flight data available to properly evaluate the range of orbital conditions and hardware implementations to be useful in validating candidate predictive methods and tools.

6.1.4 Confidence Interval: Owing to the lack of sufficient flight data to benchmark predictive efforts, it is very difficult to assess confidence intervals for on-orbit rate predictions. We recognize there are uncertainties associated with the environment description, with test data and its interpretation, and with the predictive techniques that all affect the precision with which rates can be predicted. With respect to the techniques, the worst case upper bound should provide a true limiting rate, and it may over predict the actual observed rate by orders of magnitude in some cases (e.g., high optical powers where indirect mechanisms dominate). The critical charge analysis should be good to within a factor of ~5 to 10 or better, provided it is carried out with an appropriate tool to treat both direct and indirect mechanisms and with accurate determination of critical charge. Full up testing and folding of the response function with the environment should improve accuracy to within a factor of 2 to 5, but this is only an educated guess. Also, there is no way to assess whether the rate will be over predicted or underpredicted, unless conservative approaches are used in defining the inputs.

6.2 Status and Recommendations for Optocouplers: Sections 2.2 and 3.2 described the physical mechanisms of proton interactions with high bandwidth receivers and the published suggested approaches for error rate prediction. In this section, we will provide a closer examination of the current state of our ability to take a generalized approach to optocoupler single event testing and error rate prediction. We will begin by examining currently available technology and development trends, then examine test needs and fidelity of prediction attempts with flight data, and conclude with recommendations for prediction approaches with additional comments on uncertainty. To some extent, the accuracy required in the prediction by a given application will dictate the level of effort in testing and rate prediction. So as with FOL receivers, we will attempt to indicate where shortcuts to bounding calculations may be appropriate, as well as methods required where more precision is needed.

6.2.1 Optocoupler Technology Trends and Tool Requirements: We have already discussed the COTS orientation and hybrid-related control and tractability issues associated with many optocoupler suppliers. With much recent attention given to failure and single event transient issues, there is a (slowly) growing base of vendors who are giving some attention to product needs for satellites. Consequently, there may be more choices in the future that incorporate single event tolerant components such as GaAs or InGaAs photodiodes. If so, this will be the exception, and we expect the mainstream to be dominated by Si photodetectors fabricated monolithically in modern bipolar processes. Consequently, charge collection by both drift and diffusion will be important.

6.2.2 Test Needs and Recommendations for Optocoupler Error Rate Prediction: There are obviously strong parallels between the test needs and rate prediction issues for optocouplers with those discussed for FOLs in section 6.1.2, with the notable exception being the absence of the receiver optical power as a controlled variable. The other key distinction involves the importance of charge diffusion for the case of Si bipolar optocoupler receivers.

For optocouplers we suggest a two tiered approach to testing and rate prediction, depending on the resources available and the level of confidence needed in the prediction accuracy. Since the optocouplers measured to date do not exhibit the sensitivity to direct ionization to the extent that some FOL receivers do, we see very limited use of the proton counting regime as a bounding worst case for error rate estimation. The two approaches we describe below are based on a scoping analysis relying on estimation of critical charge and then a more detailed analysis based on extensive measurements.

Unlike FOLs, there are no optical link budget based approaches to estimate critical charge, unless a cooperative vendor can provide the necessary receiver circuit details to accomplish this through modeling. Consequently, the recommended approach would rely on test data and knowledge of the diode material and geometry. Testing with energetic protons over angles ranging from normal incidence to grazing incidence would allow determination of the baseline error rate following from the indirect mechanism, and assuming there is sensitivity to direct ionization, the angle at which the cross section shows significant increase above the indirect baseline may be used in the estimation of critical charge. This requires knowledge of the proton energy at the device, and package modification to minimize the material layers is advised. Also, it is important to use tuned as opposed to degraded energy for this purpose. Figure 33 (after [18]) shows the dramatic difference associated with this issue, and it could have significant impact on estimation of critical charge.

In addition to proton angle and LET, it is necessary to know the effective pathlength, and this requires knowledge of the diode geometry. In addition, this estimate should include a diode thickness and diameter that reflects the charge collection by diffusion of electrons. In the absence of specific information, we suggest the value of 50 microns reported in [14]. For critical charge estimation, a worst case bound could include the assumption that all charge within one diffusion length of the junction is collected. Finally, we recommend that the test data used to collect this information be acquired with appropriate circuit impedances on the output. The output loads have been shown to be critical in determining if a "glitch" on the optocoupler output will propagate as an error [2], and either realistic or worst case conditions should be implemented in the test circuit.

Table 3: Test and Predictive Model Input Requirements for Optocouplers

| | Critical Charge Estimate | Data Intensive Best Estimate |
|---|---|---|
| Diode Geometry | x | x |
| Diffusion Length | x | x |
| Diode Material | x | x |
| Critical Charge | x | |
| *In-situ* Circuit Analysis | x | x |
| Measured σ vs Proton Angle | | x |
| Measured σ vs Proton Energy | | x |
| Measured σ vs Effective LET | | x |

| | | |
|---|---|---|
| DUT to DUT Variation | | x |
| Estimated Prediction Error | ~5x to 10x | ~2x to 5x |

Once the critical charge has been estimated, rate prediction can proceed as with the analogous problem discussed for FOLs in Section 6.1.2. Again, we caution that the CRÈME-96 tools may have significant limitations, but the discrepancies in the low charge regime for the proton counting case are less important for optocouplers. Here again, the preferred approach would be with NOVICE or an equivalent tool that would treat the transport of the shielded spectrum of particles with accurate energy deposition calculations in the diode geometry. At present, no tool exists that incorporates the physics of charge diffusion, so for rate prediction purposes we recommend definition of a geometry that includes one diffusion length beyond the depleted junction (or 50 microns if no additional information is available). Since optocouplers exhibit sensitivity to direct ionization only at near grazing incidence, it is important to either exercise a calculation tool (e.g. NOVICE, or FLUKA) that incorporates nuclear elastic and inelastic based energy deposition, or construct the rate as a sum of direct and indirect mechanisms as described in Section 4.3.3.

Table 3 summarizes issues associated with the critical charge approach and also indicates the important variables if requirements for higher precision in the rate predication dictate more extensive test efforts. For these efforts, we strongly recommend that the optocoupler package be opened so that the receiver photodiode can be exposed without beam transport through packaging materials. Note that the LED and full-up operation are not required for these tests, since only receiver output pulses are measured (with associated loads). Proton testing at multiple energies is required, with sweeps around grazing incidence at each energy. From this, the higher energy normal incidence tests can be interpreted with one of the indirect mechanism tools described in Section 4.1, and the direct ionization sensitivities can be determined with one of several approaches described in Section 4.2. If sufficient data at low energies are measured, the empirical prediction approach described in [14] may be possible. Alternatively, the error cross section versus effective LET can be approximated as a Weibull or other function, and the integration with the environment accomplished with NOVICE, or CRÈME-96, but with the usual cautions. The CRÈME assumption that LET is constant across the diode geometry is definitely at issue for the long pathlengths across optocoupler photodiodes, and would lead to underestimation of the higher charge deposition events. As before, geometries for input into the rate calculations should assume a significant diffusion length. Also, measurements on a statistically significant number of DUTs should be made because of the reported part-to-part variability in the response (Figure 8, and [18]).

6.2.3 Comparison with Flight Data: The situation with available flight data for optocouplers is even bleaker than with FOL receivers. There have been no successful efforts to combine a thorough test program and rate prediction effort with an adequately instrumented flight test. Comparisons with test based predictive approaches and flight data were first reported by Reed, et al., in [2] for anomalies observed in an HP6651 optocoupler flying on the Hubble Space Telescope NICMOS instrument. Predictions were made based on critical charge and using the IRPP techniques and the CRÈME-96 tool set, and agreement appeared to be within a factor of 2. This (fortuitously) corresponded to a critical charge well above the regime where the CRÈME and NOVICE comparisons diverge at low energy deposition rates (as with the SAMPEX FOL case of Section 6.1.3). In general we would not expect such good agreement.

The most significant (and only other) published comparison of predicted rates with flight data were reported in [18]. In this case, the data set was considerably more extensive with 135 errors

analyzed on the Agilent HPCL 5231. In this case, testing was done in the application circuit configuration, and data were acquired versus energy and angle for protons and with heavy ions in an attempt to fully describe the cross section trends with effective LET (see Figure 15 after [18]). Weibull fitting of the data and use of the CRÈME-96 routine led to predicted rates of 20 per day versus 7 per day observed. This agreement of within a factor of 3 was considered to be good, and the events included a mix of proton hits in the SAA and others at higher inclinations of the 705 km, 98 degree inclined orbit of the TERRA satellite. Of the total 135 events, all but 30 were reported within the SAA. Of those 30, 23 corresponded to the 14 July, 2000 "Bastille Day" solar particle event. 70% of the total were predicted by the CRÈME-96 and Weibull method to occur from direct ionization and 30% were expected from the prediction based on indirect mechanisms using the Bendel treatment [18].

In [18], the authors also provide a comparison between predicted rates using the CRÈME-based IRPP approach with the empirical approach of [14] for a 6N134, and the two methods show very similar results, though no flight data are available to support these predictions.

6.2.4 Confidence Interval: We recognize that there are several sources of uncertainty both with the critical charge estimation rate prediction and also with the more data intensive approaches. Reliance on critical charge determination at near grazing incidence and uncertainties on diffusion length are especially tricky, and consequently the precision of the critical charge based prediction is considered to be roughly order-of-magnitude. Uncertainty can be minimized if care is taken to control the test input variables, and additional high energy proton testing has been shown to be very effective in improving the knowledge of the threshold LET and critical charge as illustrated in Figure 6 (after [2]).

Uncertainties associated with the test data intensive approach include the usual sources related to the environment, part to part variability, and the role of diffusion as previously discussed. In addition, the presence of low energy protons in the shielded environment will factor into the emphasis that should be placed of gathering test data at low energies. Even with delidded parts, proton range issues at low energies complicate the testing and increase uncertainties. Since the observed rates may be dominated by these lower energy protons, we optimistically estimate the uncertainties to be somewhere in the range of 2 to 5x. As more combinations of test and flight come available, we hope to reduce these uncertainties significantly.

6.3 Applicability to Other Semiconductor Detectors: In principle, the techniques and tools described here can be applied to other detectors such as p-n diode arrays, charged coupled devices (CCDs), APDs, CMOS sensors, etc., but with cautions according to the two general cases below. Also, we note that the energy deposition problem addressed here for photodiodes is limited to the photocurrents collected in the device, gain and other effects in detector readout circuitry should not be overlooked.

6.3.1 Imagers with full depletion: This represents the simpler case, and the determination of charge deposition relies on the proper determination of the LET and pathlength distributions, along with the ionization potential specific to the detector material. Tools described above such as NOVICE are fully capable of first order estimates of pixel hit rates above a given charge level, but additional steps are required to assess the effects of secondary particles and the temporal and spatial correlation issues that may be important to imaging sensors. At present, assessment methods and tool developments are under way for specific detector materials, and the roles of MCNP-x, GIANT-4, NOVICE, and other codes are under evaluation [19].

6.3.2 Imagers with partial depletion: This case differs from the previous one only to the extent that charge diffusion from substrates or passivation layers may contribute significant charge. In addition to the series of codes required to treat the case of fully depleted imagers, rigorous evaluation of partially depleted devices requires a summing of the drift-collected charge with the diffused charge. References [20 and 21] provide discussions of the device physics and methods to accomplish this, but thus far no widely available tool exists to perform the calculations. Again, work is under way to develop these capabilities (including secondary particle and diffusion effects) for infrared imagers [19], and these developments should be monitored to assess their application to both the FOL and optocoupler transient rate problems.

7.0 Requirements and Prospects for a Unified Tool for Rate Predictions: There are definite common areas for the FOL and optocoupler rate prediction problems, and almost certainly a common tool can be devised. The areas of difference are the lower charge regime and increased number of material systems for the FOL case and the inclusion of charge diffusion for the optocoupler case. At present, no single tool exists that treats all these issues sufficiently to provide high confidence in our ability to predict error rates within a factor of 2, but order of magnitude estimates are certainly possible.

An ideal tool would accept a user defined arbitrary geometry, material composition, and ionization potential, along with a user friendly interface to either generate or import particle environment descriptions. Generation of chord distribution and transport of the input environment would lead to charge deposition event rates above a given critical charge level. Alternately, input of error cross section data via a Weibull or other user defined response function could be folded with the chord distribution and environment to arrive at an event rate. The tool should also be capable of assessing events from nuclear elastic and inelastic events. So far, all this is possible with NOVICE, and one recommendation is to explore the utility of NOVICE to both the optocoupler and FOL problems by exercising it to assess NOVICE predicted rates against flight data and other candidate prediction approaches wherever possible. Inclusion of diffusion contributions need to be explored by either modifying geometries to define effective collection depths, or by tool development to treat diffusion explicitly. Tracking progress and leveraging on the imager tool development efforts mentioned in Section 6.3 seems the best approach for now.

Issues identified with the existing CRÈME tool render it suspect for high accuracy predictions, even for Si devices. We recommend it be used only in regimes where the approximations and error sources we have discussed are understood, and then only for rough estimates. Given the popularity and general availability of CRÈME, we consider that attempts to improve its capabilities would be appropriate. The areas that need to be addressed are the anomalous results for low energy deposition events, the modification to track or approximate LET as if changes across a sensitive geometry, and the addition of other target materials to include GaAs and InGaAs with options for specifying the bandgap dependent ionization potential. Addition of RCC geometry should also be considered if CRÈME were to be modified to treat these problems.

We also recognize the needs for improved rate prediction in this class of devices is not unique to NASA. The suitability and enhancements to FLUKA and GIANT-4 have already been discussed in Section 4.1.3. We understand that the European Space Agency is interested in this problem [40], and to the extent that we have common goals there should be coordination to avoid duplication of efforts and coordinate our approaches. So a third recommendation would be to establish better communications to track ESA's interests and progress.

8.0 Conclusions and Final Comments: A comparative review of published test and flight data in fiber optic links and in optocouplers reveals minor differences in the underlying physical mechanisms and supports the claim that they have much in common. Our critical assessment of the status of methods and tools to predict particle induced error rates in both technologies indicates that we are presently limited to factor of 3-5 estimates, and then only with data intensive characterization efforts. Presently, no single tool exists that is appropriate for the full range of variables associated with these problems, but prospects are excellent for the development of a unified tool that would not only benefit these problems but also find application to related rate prediction problems in imagers and other detectors. Presently, assessments are under way to examine the suitability of tools such as GIANT-4, MCNP-x, NOVICE, and other expert level Monte Carlo based tools for various detector related SEE concerns. In parallel, assessments are being made to evaluate the role of charge diffusion and tools required to properly assess its role in bipolar microelectronic devices and in detectors. Until the related studies are completed, it is difficult to define the next step required for a unified solution to rate prediction for FOLs and optocouplers, and we recommend that the concerns unique to these FOL and optocoupler problems be critically assessed with other detector problems, and appropriate benchmark tests be defined to evaluate appropriate solutions. Unfortunately, at least in the interim, we expect that these solutions will require comparatively sophisticated computer codes with expert interactions before more user friendly tools can be made available, at least when better that order-of-magnitude estimates are desired.

9.0 Acknowledgements: The rate prediction tool assessment is only possible due to funding from the NASA Electronic Radiation Characterization Project and the Defense Threat Reduction Agency (DTRA) Radiation Tolerant Microelectronics Program. Helpful input, discussions, and suggestions from the following colleagues are also appreciated: Ken LaBel, Robert Reed, Christian Poivey, Cheryl Marshall, Brian Fodness, Steve Buchner, Ray Ladbury, Tom Jordan, Jim Pickel, Mike Xapsos, Allan Johnston, Clive Dyer, and Gordon Hopkinson.

## 10.0 References:


[1] K.A. LaBel et al., “On the Suitability of Fiber Optic Data Links in the Space Radiation Environment: Historical and Scaling Perspective,” Proc. IEEE Aerospace, Snowmass, CO, March 1998.

[2] R.A. Reed et al., “Emerging Optocoupler Issues with Energetic Particle-Induced Transients and Permanent Degradation,” IEEE Trans. Nucl. Sci., Vol. 44, No. 6, pp. 2833-2841, Dec.1998.

[3] B.G. Rax et al., “Total Dose and Displacement Damage in Optocouplers”, IEEE Trans. on Nuclear Science, Vol. 43, No. 6, pp. 3167-3173, Dec. 1996.

[4] K. A. LaBel et al., “Transient SEUs in a Fiber Optic System for Space Applications”, IEEE Trans. Nucl. Sci., Vol. 38, pp. 1546-1550, Dec. 1991.

[5] K.A. LaBel et al. "SEDS MIL-STD-1773 Fiber Optic Data Bus: Proton Irradiation Test Results and Spaceflight SEU Data," IEEE Trans. Nucl. Sci., Vol. 40, No. 6, pp. 1638-1644, 1993.

[6] K.A. LaBel et al., “Proton-Induced Transients in Optocouplers: In-Flight Anomalies, Ground Irradiation Test, Mitigation and Implications, IEEE Trans. Nucl. Sci., Vol. 44, No. 6, pp. 1885-1892, Dec. 1997.

[7] P. Marshall et al., "Charged Particle Effects on Optoelectronic Devices and Bit Error Rate Measurements on 400 Mbps Fiber Based Data Links," RADECS Conference Proceedings, September 13-16, 1993, Saint Malo, France, pp. 266-71.

[8] P.W. Marshall et al., “Particle-Induced Bit Errors in High Performance Fiber Optic Data Links for Satellite Data Management,” IEEE Trans. Nucl. Sci., Vol. 41, pp. 1958-1965, Dec. 1994.

[9] D. Thelen et al., "A Dual Rate MIL-STD-1773 Fiber Optic Transceiver for Satellite Applications," Photonics for Space Environments II, SPIE Vol., (1994).

[10] K.A. LaBel et al., “Preliminary ground test radiation results of NASA’s MPTB dual-rate 1773 experiment”, Proc. SPIE, Vol. 2811, pp. 128-135, 1996.

[11] K.A. LaBel et al., “Comparison of MIL-STD-1773 Fiber Optic Bus Terminals: Single Event Proton Test Irradiation, In-flight Space Performance, and Prediction Techniques,” RADECS Conference Proceedings, September 15-19, 1997, Cannes, France, pp. 332-338.

[12] Cheryl J. Marshall, Paul W. Marshall, Martin A. Carts, Robert Reed, Steve Baier, and Ken LaBel, “Characterization of Transient Error Cross Sections in High Speed Commercial Fiber Optic Data Links,” IEEE Nuclear and Space Radiation Effects Conference Data Workshop Record, Vancouver, BC, 2001.

[13] F. Faccio, G. Berger, K. Gill, M. Huhtinem, A. Marchioro, P. Moreira, and F. Vasey, “Single Event Upset Tests of an 80 Mb/s Optical Receiver,” IEEE Trans. Nucl. Sci., Vol. 48, No. 5, p. 1700, Oct. 2001.

[14] A.H. Johnston et al., “Single-Event Upset Effects in Optocouplers,” IEEE Trans. Nucl. Sci., Vol. 46, No. 6, p. 2867, Dec. 1998.

[15] A.H. Johnston et al., “Angular and Energy Dependence of Proton Upset in Optocouplers,” IEEE Trans. Nucl. Sci., Vol. 47, No. 6, pp. 1335-1341, Dec. 1999.

[16] R.A. Reed, Figure 4.6 in “Performance Characterization of Digital Optical Data Transfer Systems for use in the Space Radiation Environment,” IEEE NSREC Short Course, Reno NV, 1999.

[17] A.H. Johnston, et al., “Single Event Upset Effects in Optocouplers,” IEEE Trans. Nucl. Sci., Vol. 45, No. 6, pp. 2867-75, Dec. 1998.

[18] R. Reed, et al., “Assessing the Impact of the Space Radiation Environment on Parametric Degradation and Single Event Transients in Optocouplers,” IEEE Trans. Nucl. Sci., Vol. 48, No. 6, pp.2202-2209, Dec. 2002.

[19] James C. Pickel, Robert Reed, Ray Ladbury, Bernie Roucher, Paul Marshall, Bryan Fodness, and George Gee, “Modeling Radiation Induced Transients in the Next Generation Space Telescope,” Submitted to the IEEE Aerospace Applications Conference, March 2002.

[20] T.S.Lomheim, R.M.Shima, J.R.Angione, W.F.Woodward, D.J.Asman, R.A.Keller and L.W.Schumann, "Imaging Charge-Coupled Device (CCD) Transient Response to 17 and 50 MeV Proton and Heavy Ion Irradiation," IEEE Trans. Nucl. Sci., Vol. 37, No. 6, p. 1876, December 1990.
[21] T.E.Dutton, W.F.Woodward and T.S.Lomheim, "Simulation of Proton-Induced Transients on Visible and Infrared Focal Plane Arrays in a Space Environment, SPIE, Vol. 3063, p.77, 1997.
[22] S.Kirkpatrick, "Modeling Diffusion and Collection of Charge from Ionizing Radiation in Silicon Devices," IEEE Trans. Elec. Dev., Vol. ED-26, p. 1742, 1979.
[23] T.M.Jordan, "An Adjoint Charged Particle Transport Method," IEEE Trans. Nucl. Sci., Vol. 23, 1976.
[24] http://crsp3.nrl.navy.mil/creme96/
[25] A. Fasso, et al., Proc. IV Int. Conf. on Calorimetry in High Energy Physics, Sept. 20-25, 1993, p. 493.
[26] Ed Petersen, "Single Event Analysis and Prediction," IEEE Nuclear and Space Radiation Effects Conference Short Course, Snowmass, CO, 1997.
[26a] A.J. Tylka, W.F. Dietrich, P.R. Boberg, E.C. Smith, and J.H. Adams, Jr., "Single Event Upsets Caused by Solar Energetic Heavy Ions," IEEE Transactions on Nuclear Science, NS-43, No. 6, Dec. 1996.
[27] Pete Truscott, et al., "GIANT-4: A New Monte Carlo Toolkit for Simulating Space Radiation Shielding and Effects," IEEE Nuclear and Space Radiation Effects Data Workshop Record, Reno NV, p. 147, 2000.
[28] http://www.spenvis.oma.be/spenvis/
[29] http://www.spenvis.oma.be/spenvis/help/models/upseto/upsetomain.html
[30] Pickel, J. C., and J. T. Blandford, Jr., Cosmic-Ray-Induced Errors in MOS Devices, IEEE Trans. Nucl. Sci., NS-27, 1006-1015, 1980.
[31] Private Communication, Tom Jordan of EMP, also see: http://see.msfc.nasa.gov/see/ire/model_novice.html
[32] D. Binder, "Analytic SEU Rate Predictions Compared to Space Data," IEEE Trans. Nucl. Sci., NS-35, p. 1570, (1980).
[33] T. M. Scott, "A Single Event Rate Calculation Technique," IBM Report 89-PN6-004, Feb. 1989.
[34] Kenneth A. LaBel, "Applying State of the Art (SOTA) Commercial and Emerging Technologies to Space Systems," IEEE Nuclear and Space Radiation Effects Conference Short Course Notes, Newport Beach CA, July 20, 1998.
[35] Xiaoli Sun and Henri Dautet, "Proton Radiation Damage on Si APD Single Photon Counters," IEEE Nuclear and Space Radiation Effects Conference Data Workshop Record, Vancouver, BC, July 2001.
[36] Private communication with Tom Jordan, Engineering and Mathematical Physics Consultants, Gaithersburg, MD.
[37] Martin E. Fritz, Glenn Berg, Dan A. Cross, and Maurice C. Wilkinson, Photonics Space Experiment On-Orbit Results, SPIE Vol. 2811, p. 106, August 1996.
[38] George L. Jackson, Kenneth A. LaBel, Mark Flanegan, Cheryl, Dale, Paul W. Marshall, Rodney K. Bonebright, Jae H. Kim, Eric Y. Chan, Thomas M. Bocek, and Charles White, The Microelectronics and Photonics Test Bed Dual Rate 1773 Fiber Optics Data Bus Experiment, SPIE Vol. 2811, p. 116, August 1996.
[39] L. Jackson, Kenneth A. LaBel, Cheryl, Dale, Janet Barth, John Kolasinski, Chris Seidleck, and Paul W. Marshall, "Preliminary Flight Results of The Microelectronics and Photonics Test Bed NASA Dual Rate 1773 (DR1773) Fiber Optics Data Bus Experiment, GOMAC Digest, 1999.
[40] Private communication with Clive Dyer.

11.0 Figures:

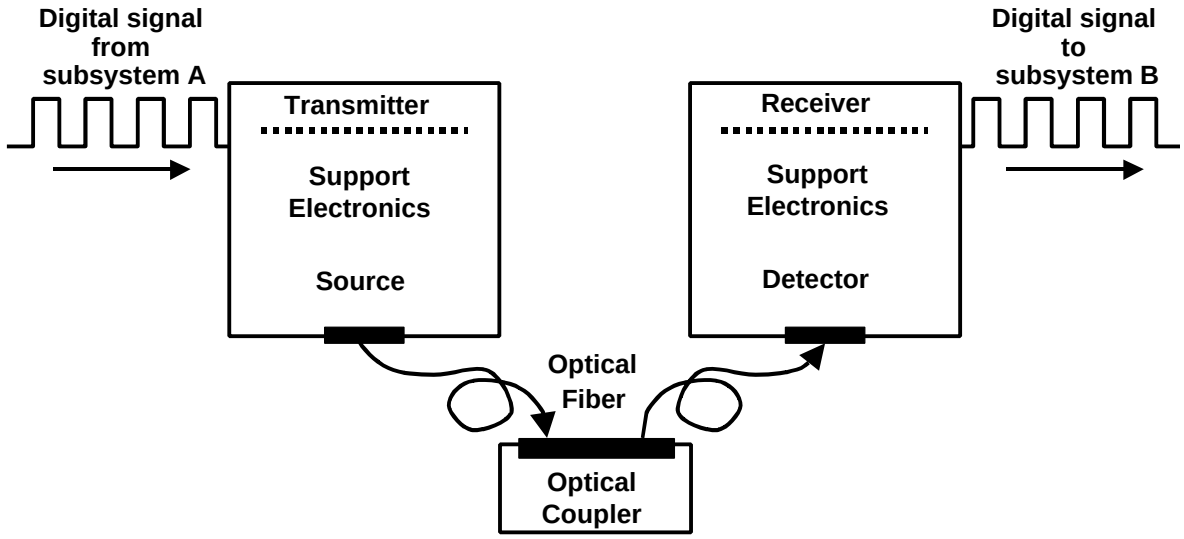


Figure 1a. Typical fiber optical link architecture.

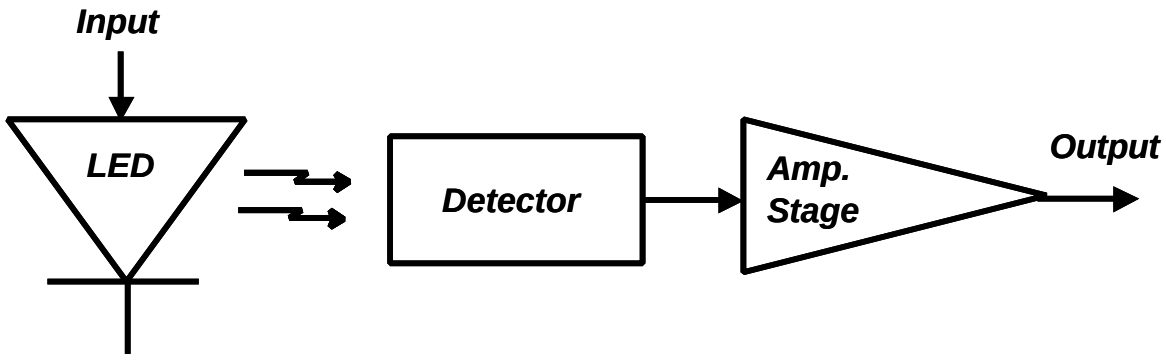


Figure 1b. Typical Optocoupler design.

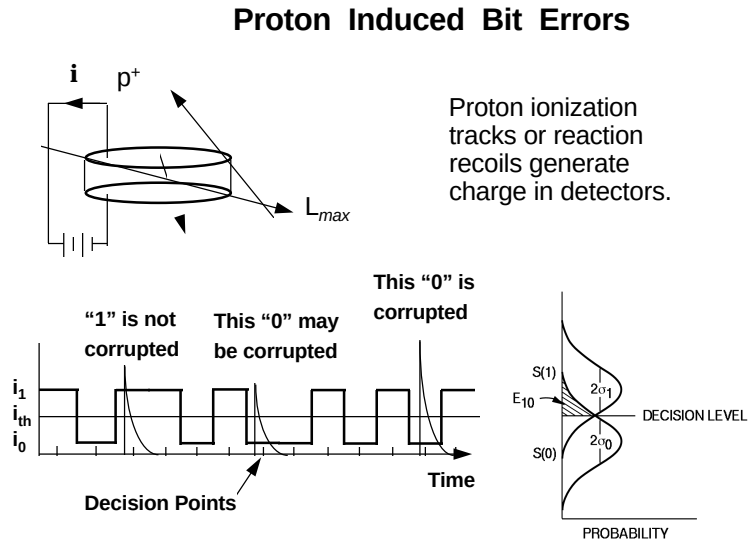


Figure 2. Proton ionization in receiver photodiodes induces photocurrents which may disrupt data. This figure is reproduced from [8].

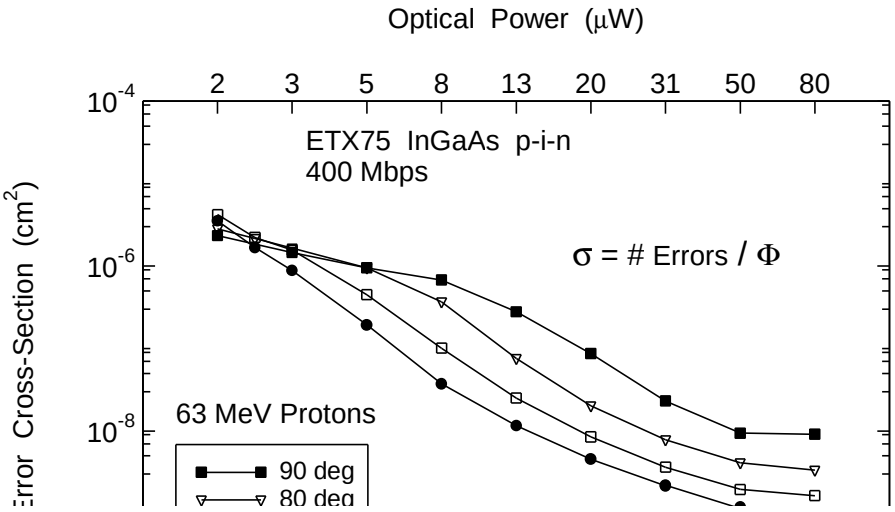


Figure 3. Proton-induced error cross-sections vary strongly with optical power and depend on particle angle. This figure is reproduced from [8].

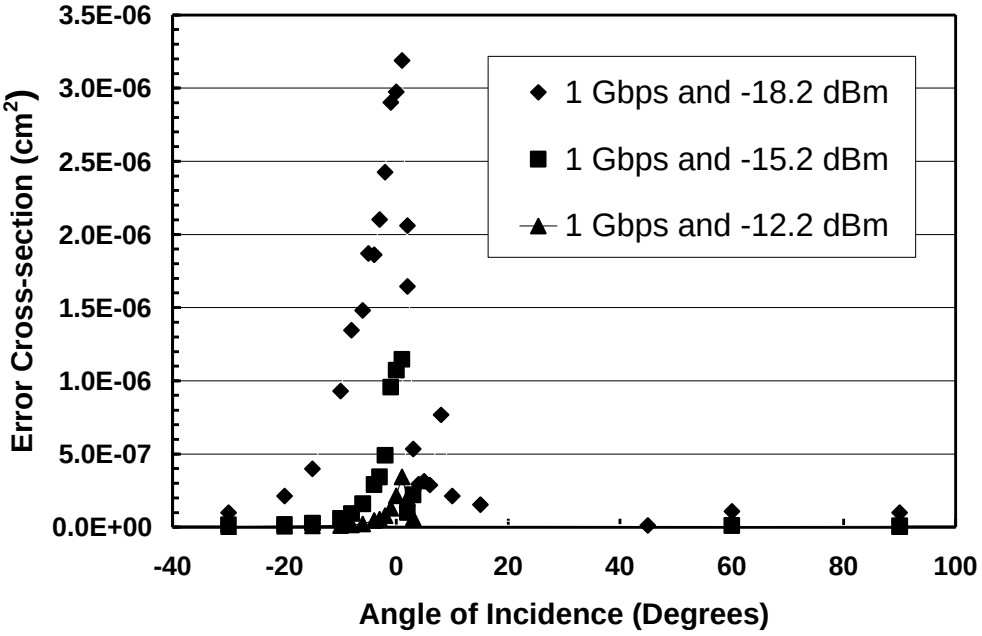


Figure 4. The dramatic increase in error cross section versus incidence angle is present at all levels of incident optical powers in this fiber optic data link. At zero degrees, the proton traverses the plane of the detector and the maximum path length is obtained.

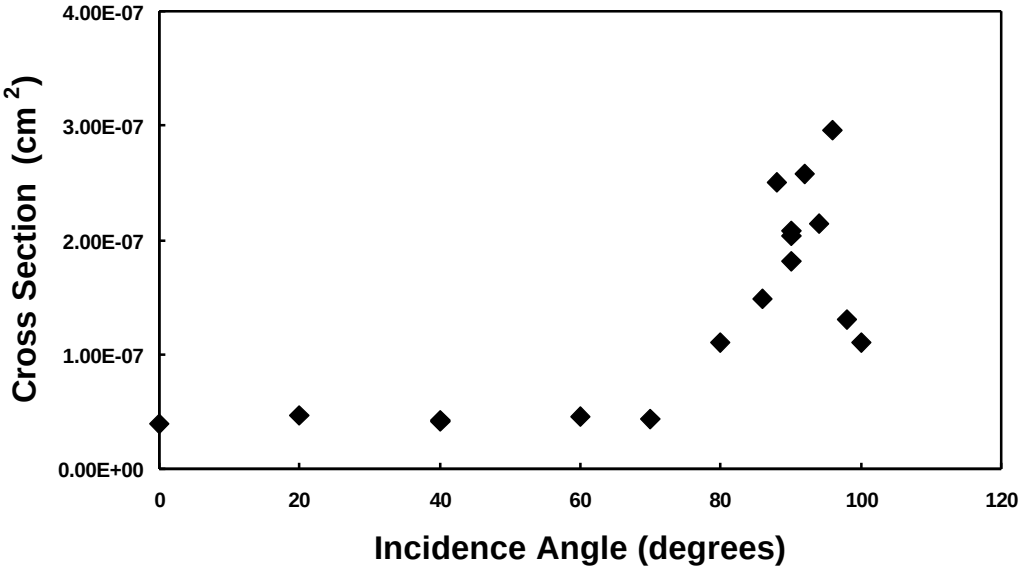


Figure 5. The order of magnitude increase in proton transient cross-section at grazing incidence is evidence of the direct ionization mechanism in the optocoupler photodiode [after 6]. The device is an HP6651.

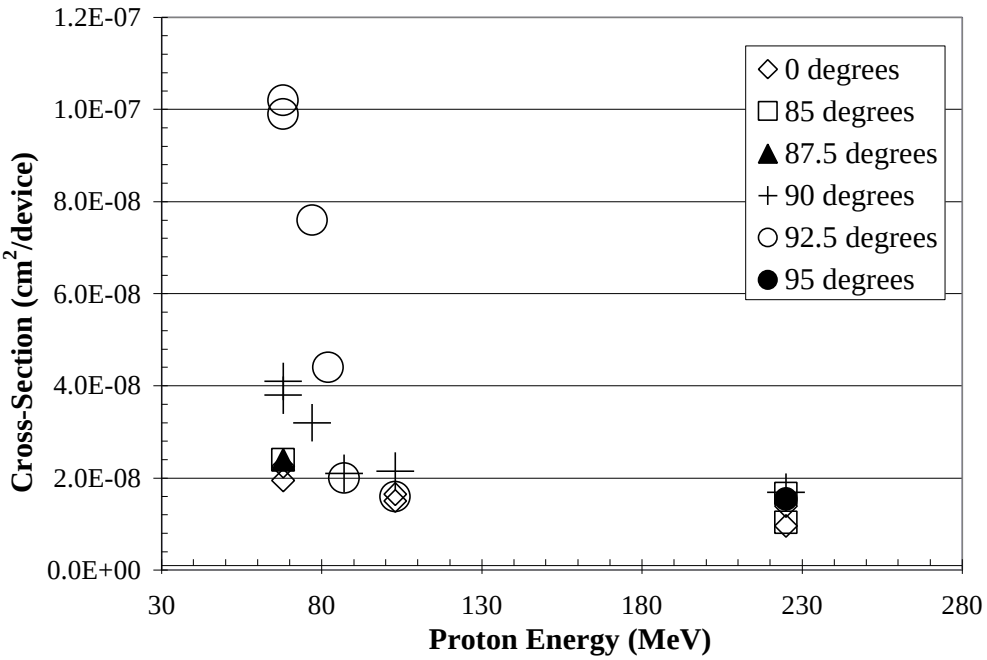


Figure 6. The transient cross section for normal incidence does not vary strongly with energy above 60 MeV, but the enhanced sensitivity to grazing angle trajectories is only seen at the lower proton energies.

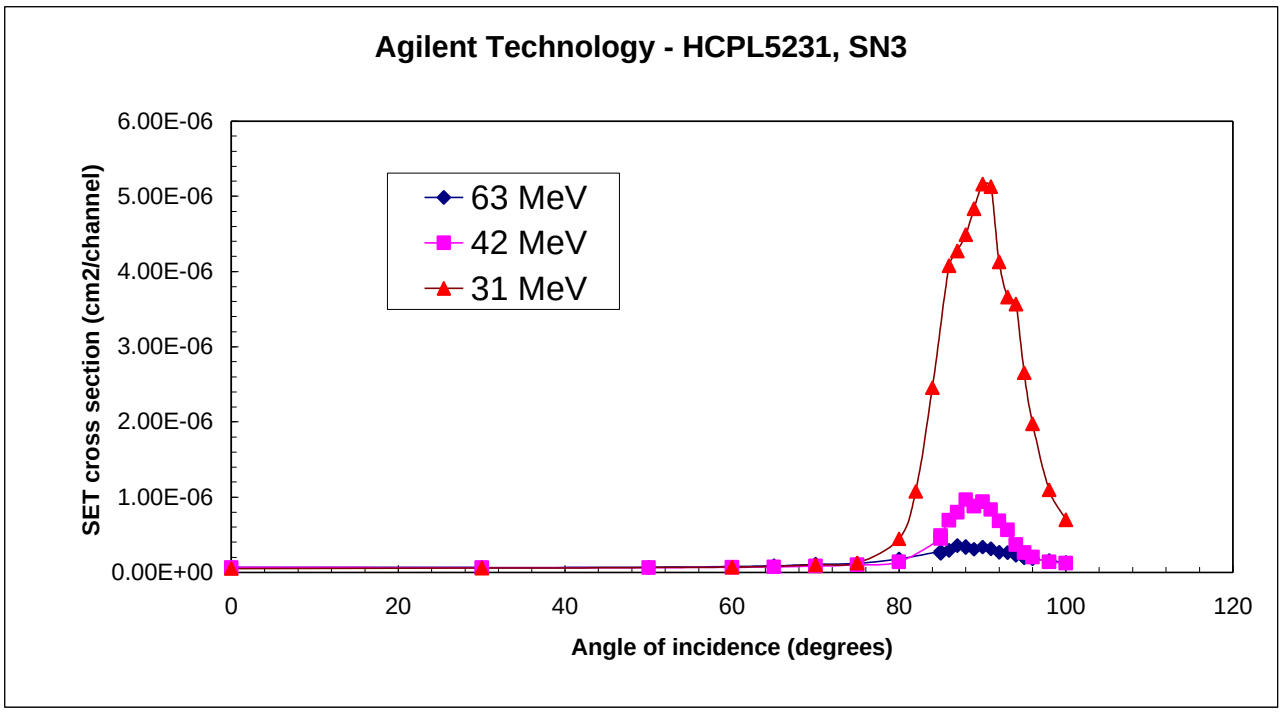


Figure 7. The effect of incidence angle on cross section for the Agilent HCPL5231 optocoupler at various proton energies [after 18].

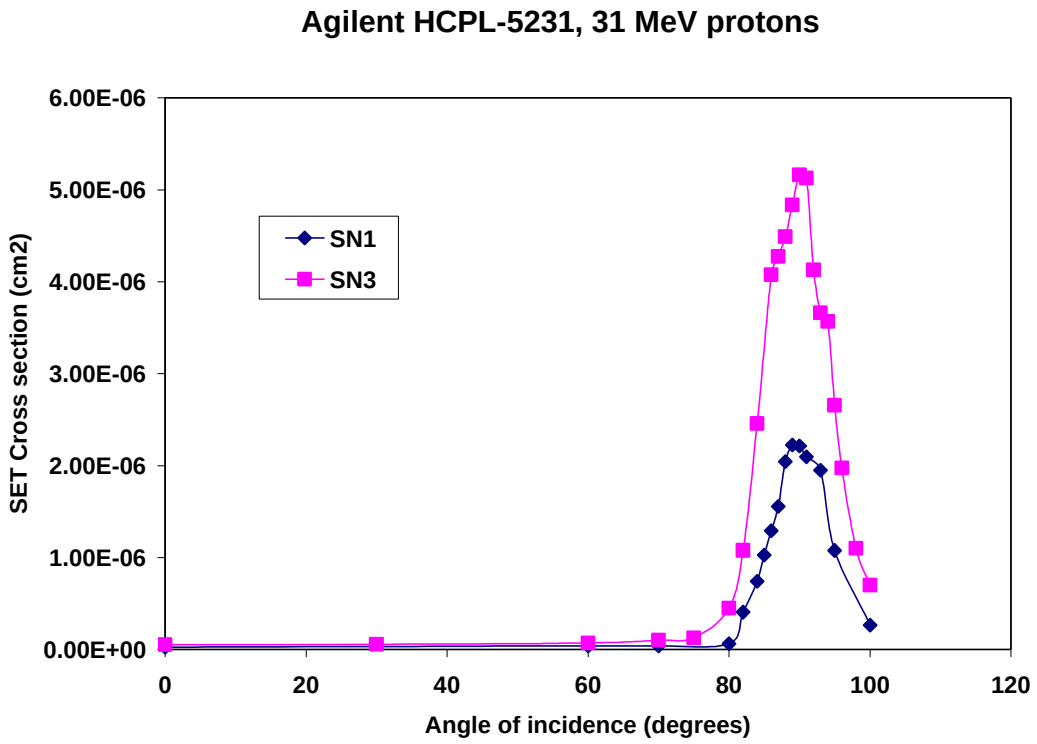


Figure 8. Example of part to part dispersion observed during proton SET characterization of the Agilent HCPL5231 [after 18].

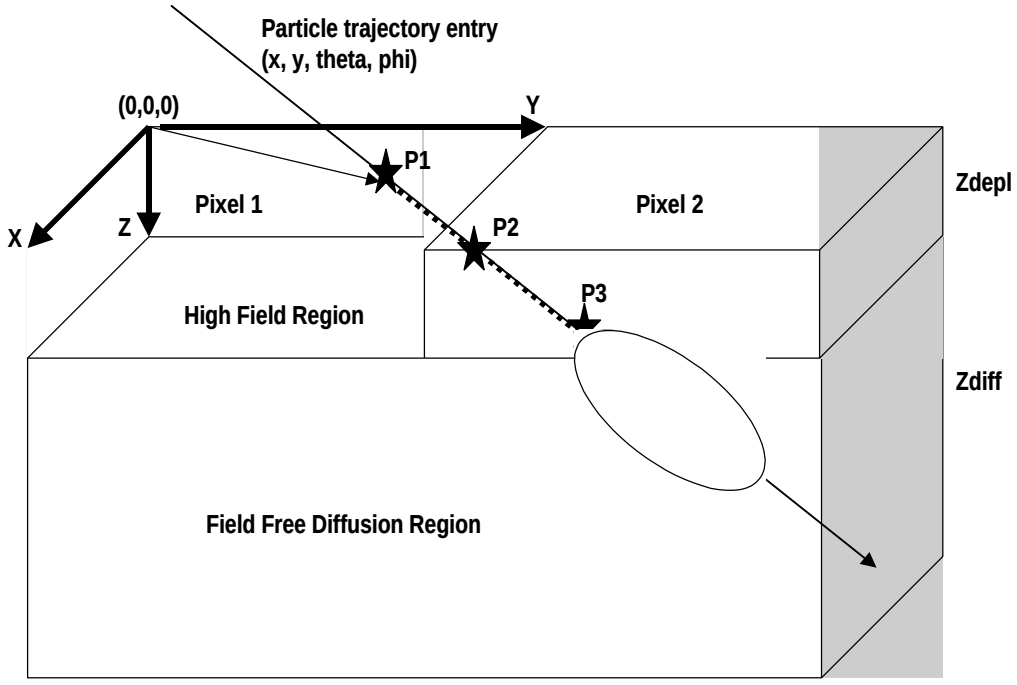


Figure 9. Illustration of Array Charge Model. A particle passes through depletion regions in pixel 1 from P1 to P2, and pixel 2 from P2 to P3 and then passes into the common substrate diffusion region [after 19].

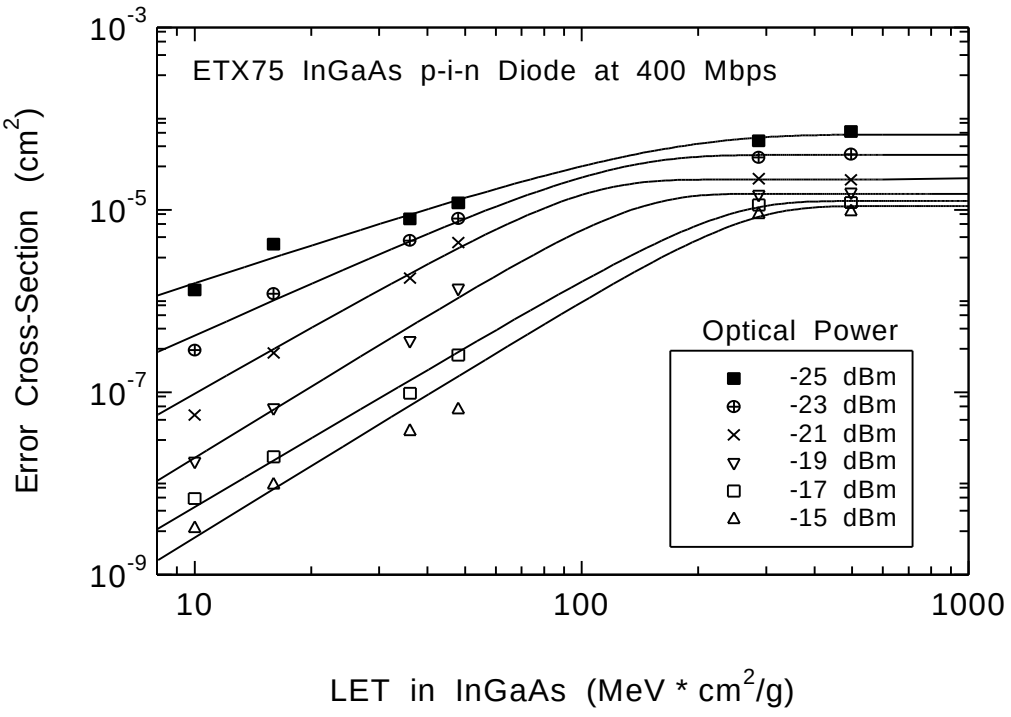


Figure 10. For protons of various angles and energies incident on a 75 micron diameter InGaAs p-i-n photodiode, Weibull distributions approximate the cross-section with LET trends.

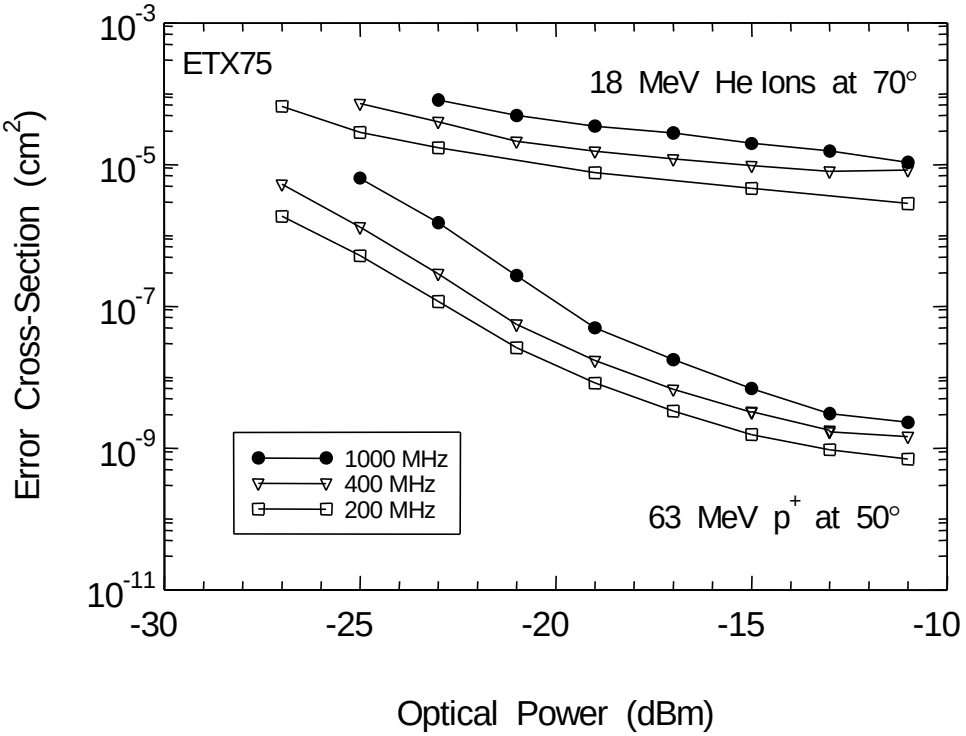


Figure 11. For the highest and lowest LET ions used in the study of errors in a 75 micron diameter InGaAs p-i-n detector with receiver AGC circuitry, the cross-section scales approximately with data rate irrespective of the link's optical power.

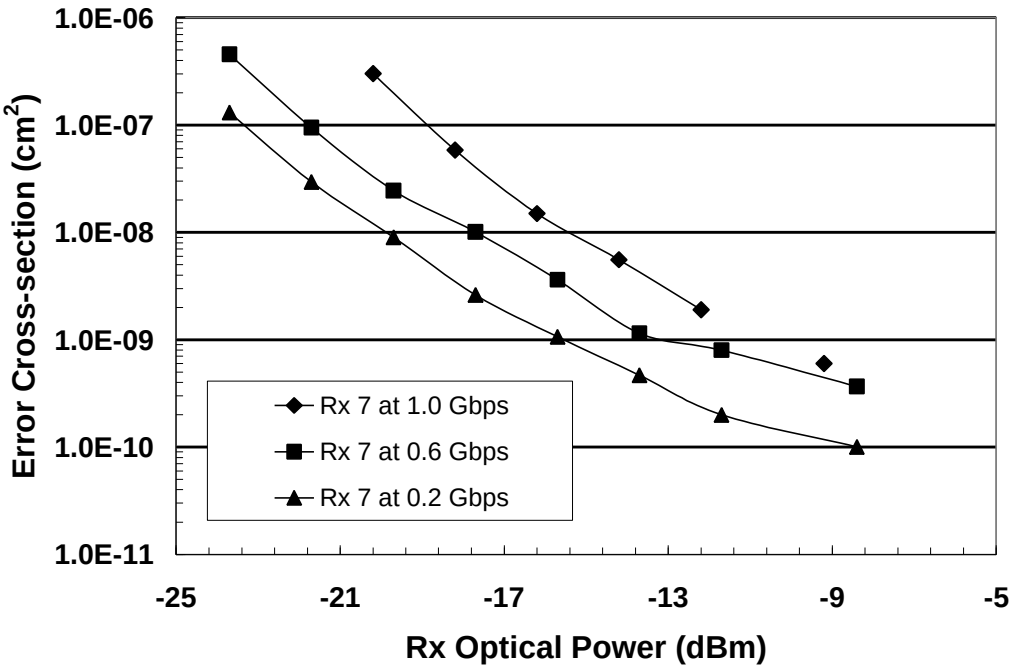


Figure 12. The error cross section decreases dramatically with increasing optical power, and increases with increasing data rate. This trend is exploited to mitigate the on-orbit bit error rate.

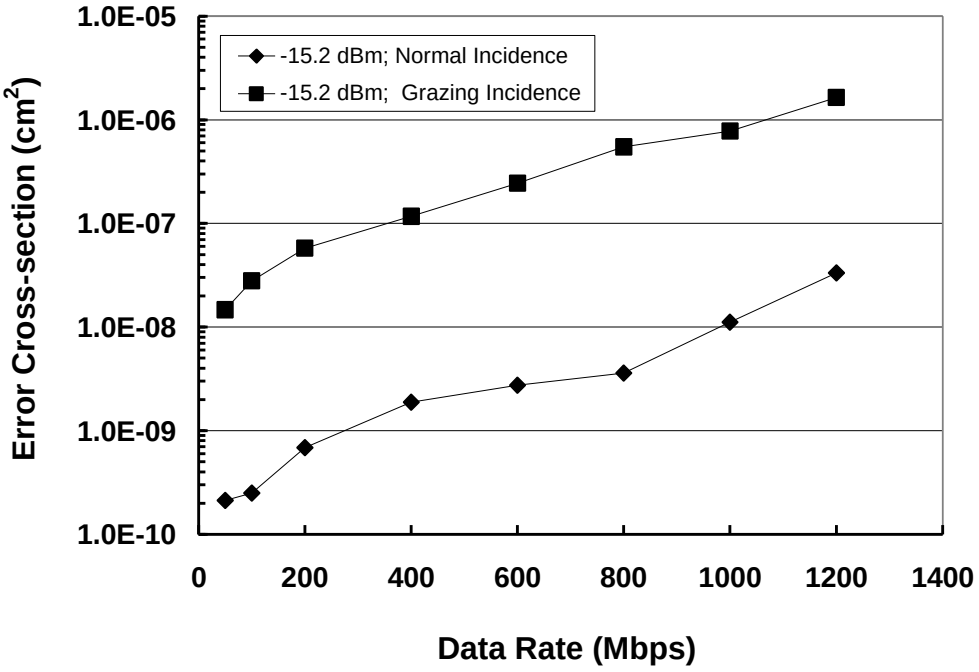


Figure 13. The trend of increasing error cross section with data rate is expected, but we do not know a reason for the greater-than-linear increase. Similar trends were observed for both normal and grazing incidence angles in the Honeywell Ruggedized Link® with AGC based receiver.

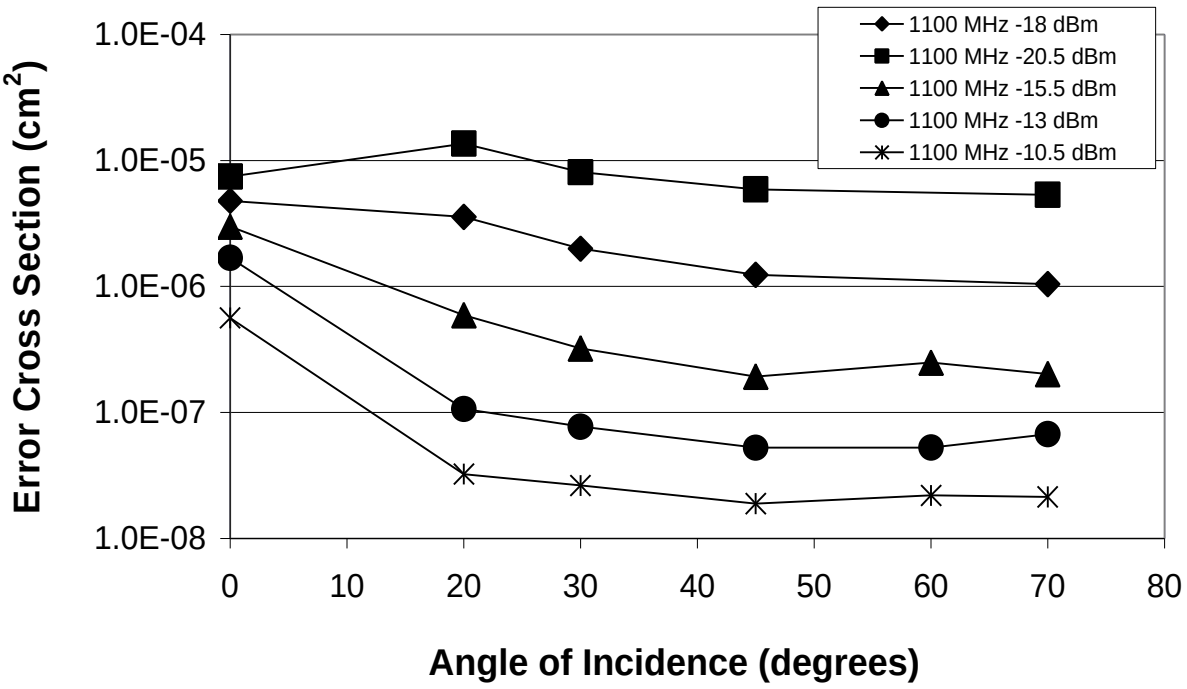


Figure 14. HP HFBR-53DE transceiver bit error cross section versus incident proton angle and optical power [after 12]. Note the difference in trends with incidence angle depending on the operating optical power.

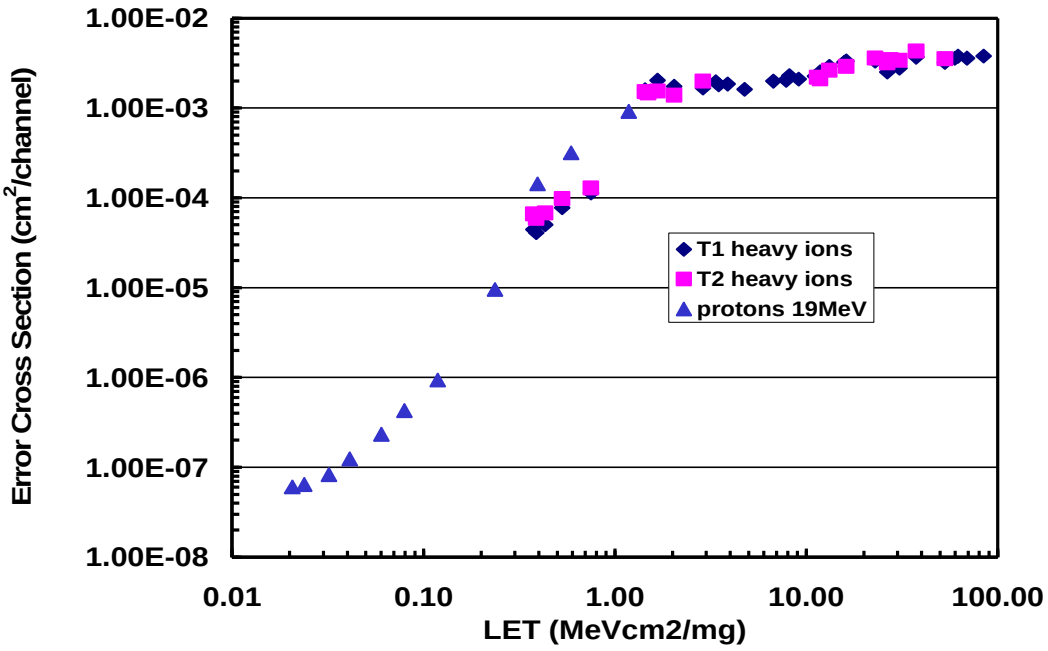


Figure 15. Proton and heavy ion error cross section measurements on an Agilent HCPL5231 optocoupler show a smoothly varying trend described by effective LET from protons and various heavy ions.

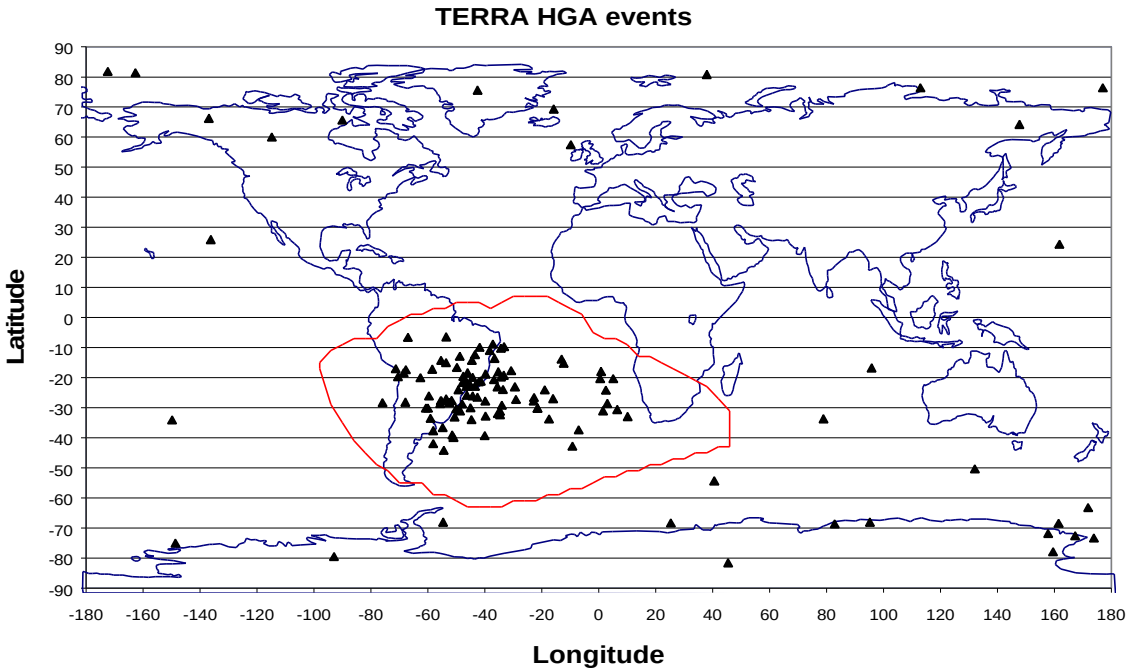


Figure 16. Mercator map projection of observed HCPL-5231 optocoupler errors show a higher density of hits in the proton rich South Atlantic Anomaly, and also at extremes in latitude for a 690 km x 98 degree circular orbit.

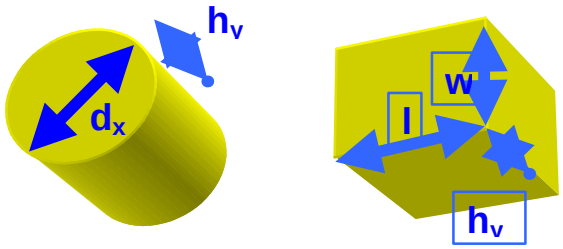


Figure 17. NOVICE calculations of the exact chord lengths for right circular cylinders are compared to that of rectangular parallelepipeds with equal surface area.

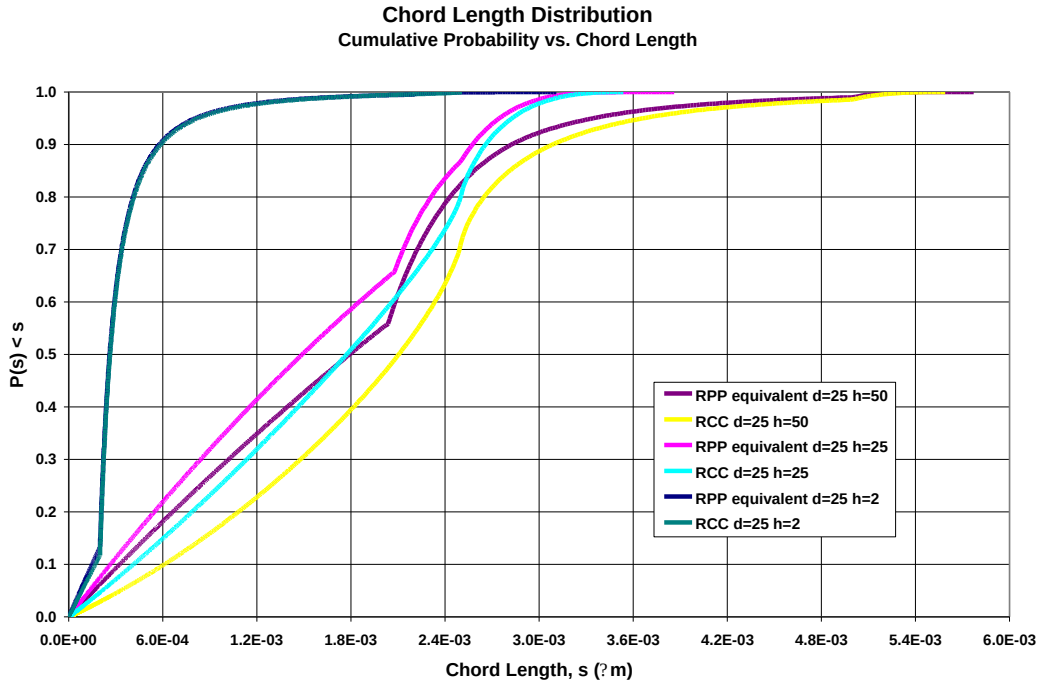


Figure 18. Comparisons of IRCC versus IRPP chord length distributions are made for cylinders with 25 micron diameter and heights of 2, 25, and 50 microns. Corresponding aspect ratios are 12.5, 1.0, and 0.5.

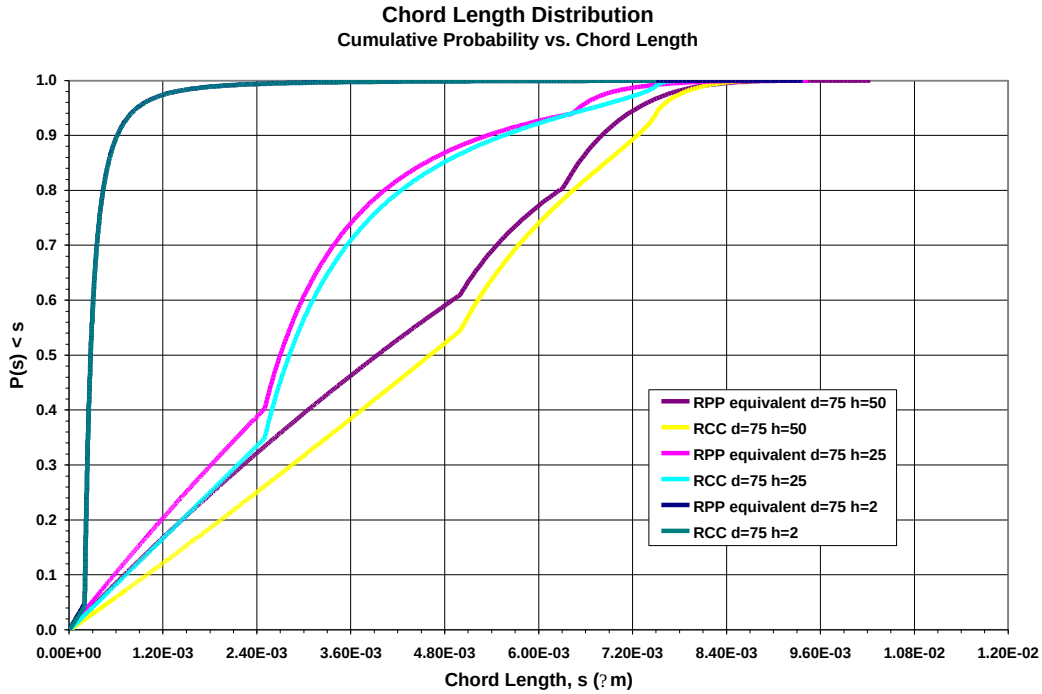


Figure 19. Comparisons of IRCC versus IRPP chord length distributions are made for cylinders with 75 micron diameter and heights of 2, 25, and 50 microns. Corresponding aspect ratios are 37.5, 3.0, and 1.5.

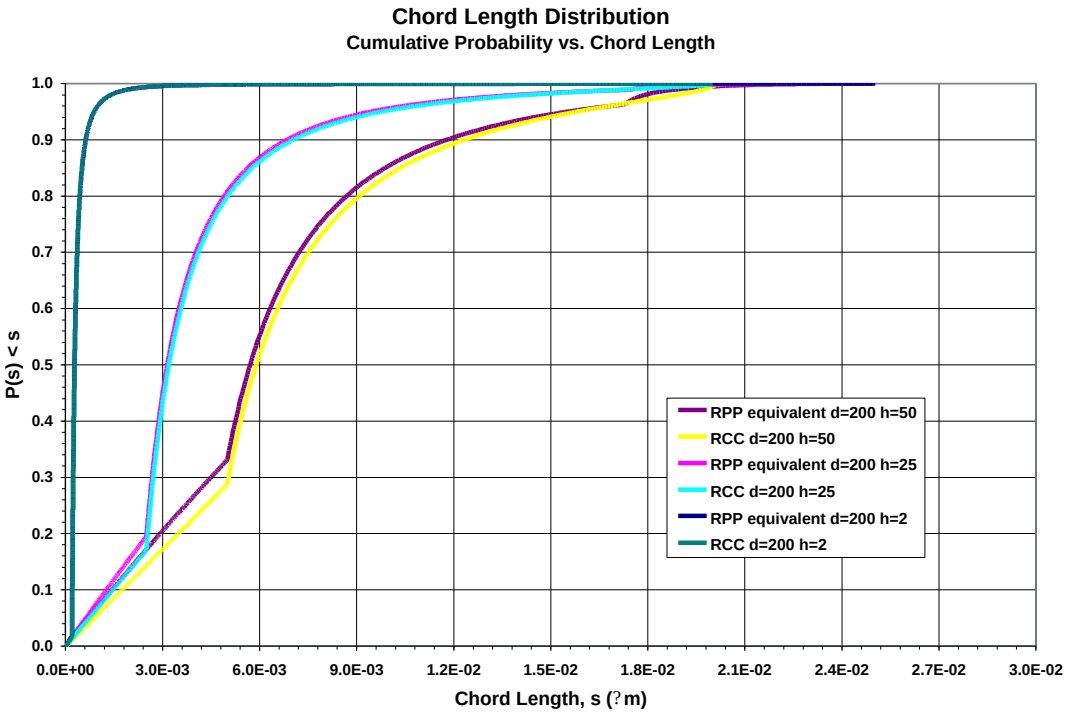


Figure 20. Comparisons of IRCC versus IRPP chord length distributions are made for cylinders with 200 micron diameter and heights of 2, 25, and 50 microns. Corresponding aspect ratios are 100, 8.0, and 4.0.

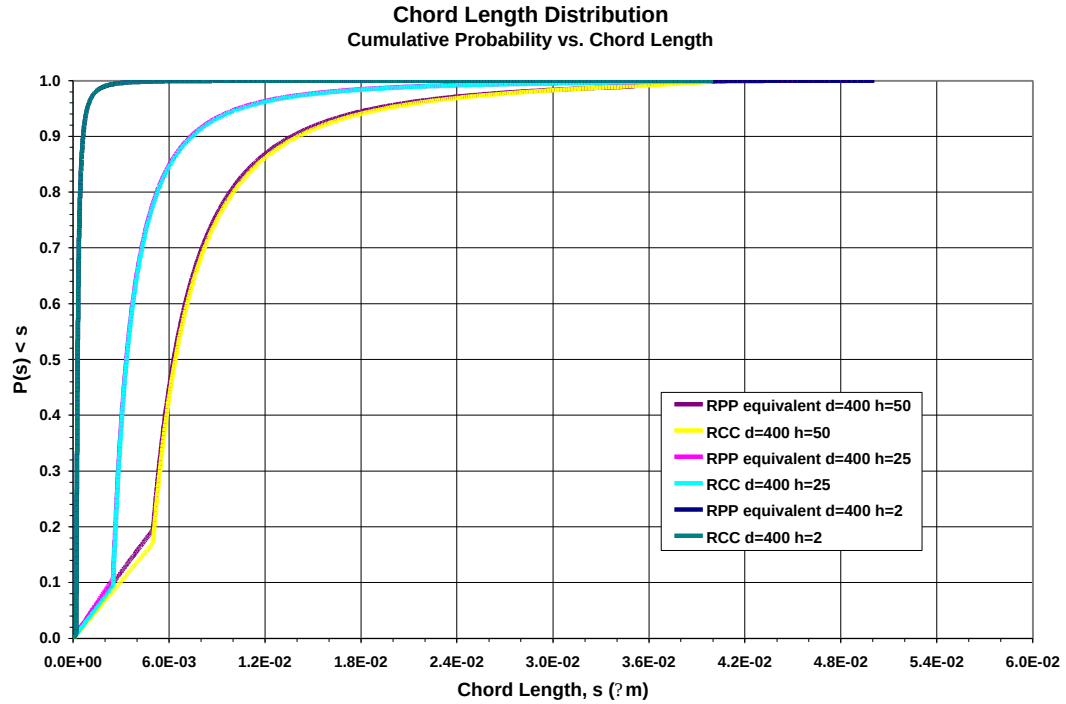


Figure 21. Comparisons of IRCC versus IRPP chord length distributions are made for cylinders with 400 micron diameter and heights of 2, 25, and 50 microns. Corresponding aspect ratios are 200, 16.0, and 8.0.

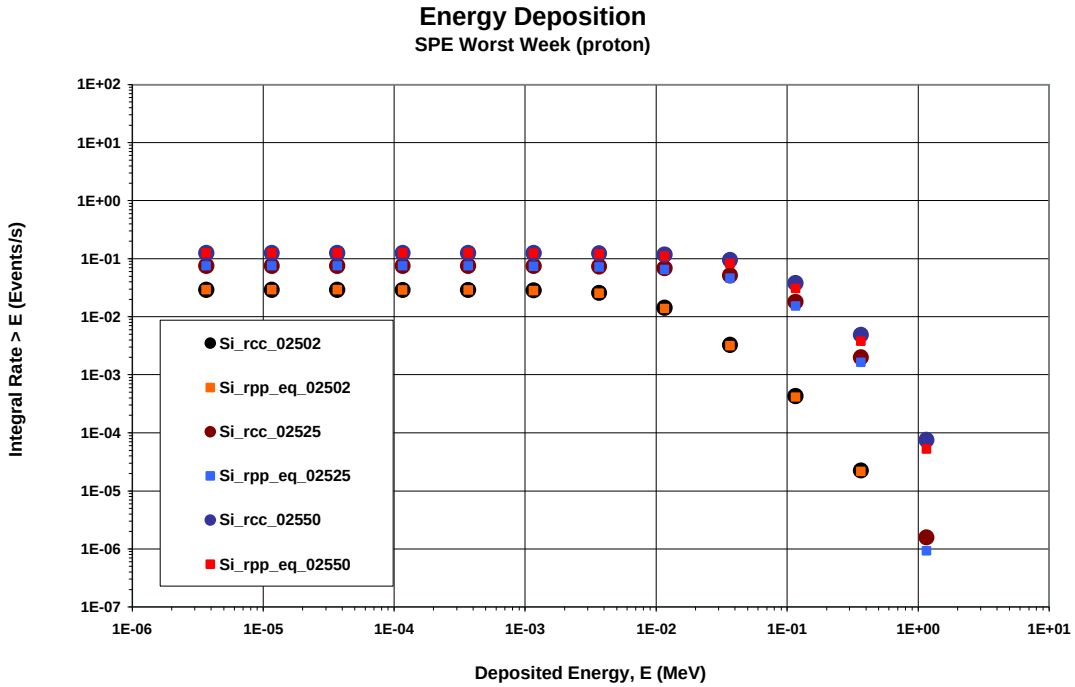


Figure 22. Comparisons of IRCC versus IRPP proton energy deposition distributions in Si are made for cylinders with 25 micron diameter and heights of 2, 25, and 50 microns. Corresponding aspect ratios are 12.5, 1.0, and 0.5.

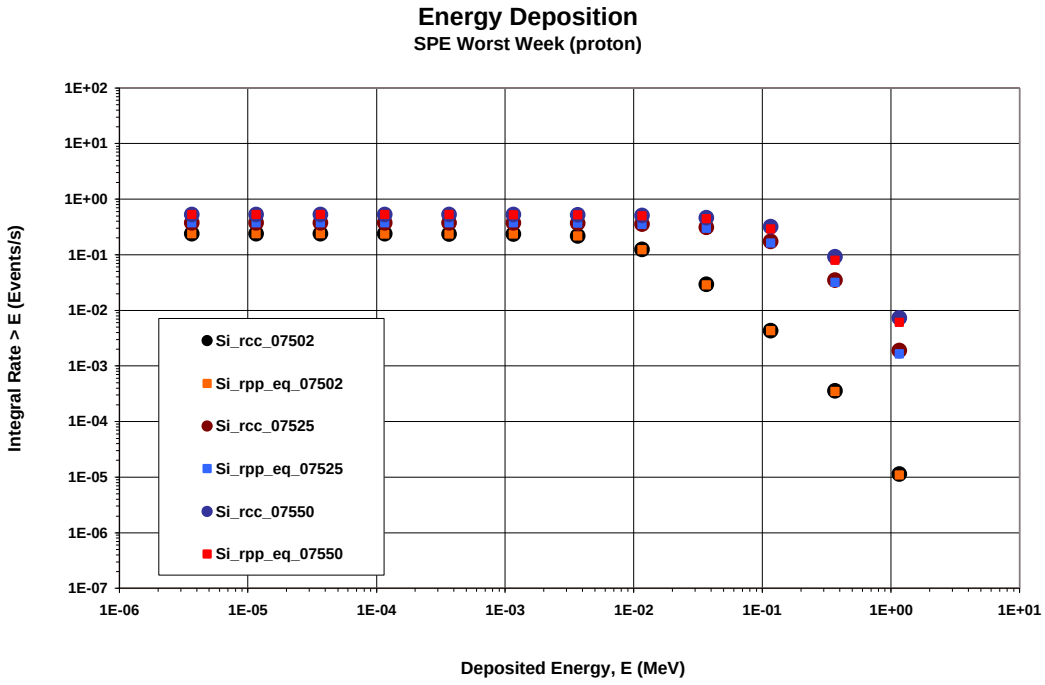


Figure 23. Comparisons of IRCC versus IRPP proton energy deposition distributions in Si are made for cylinders with 75 micron diameter and heights of 2, 25, and 50 microns. Corresponding aspect ratios are 37.5, 3.0, and 1.5.

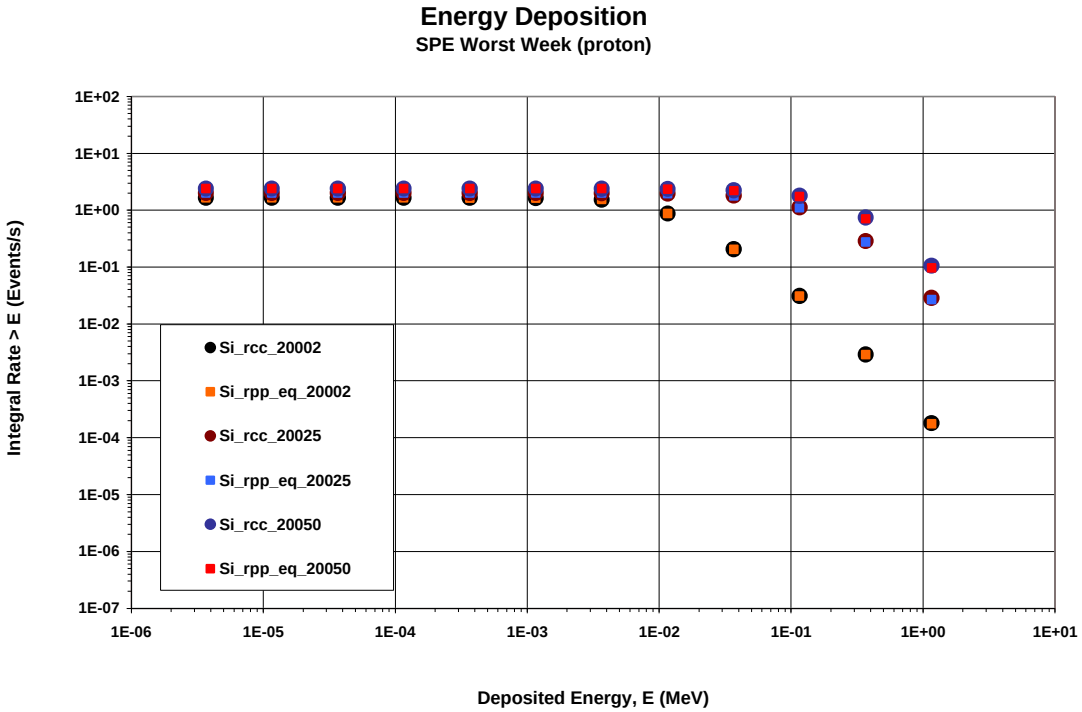


Figure 24. Comparisons of IRCC versus IRPP proton energy deposition distributions in Si are made for cylinders with 200 micron diameter and heights of 2, 25, and 50 microns. Corresponding aspect ratios are 100, 8.0, and 4.0.

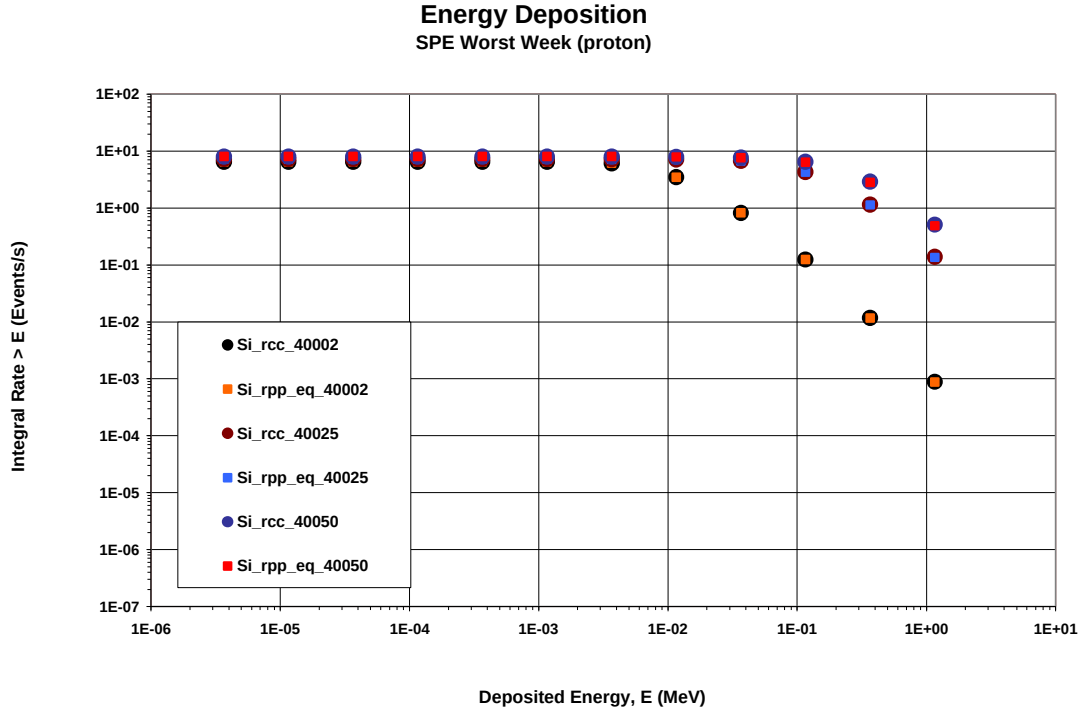


Figure 25. Comparisons of IRCC versus IRPP proton energy deposition distributions in Si are made for cylinders with 400 micron diameter and heights of 2, 25, and 50 microns. Corresponding aspect ratios are 200, 16.0, and 8.0.

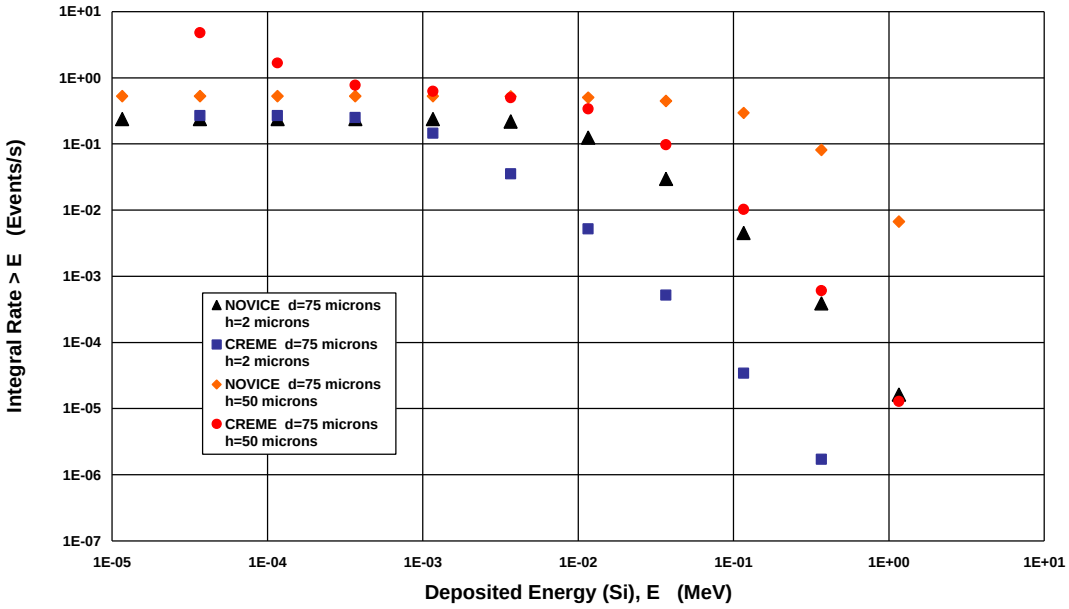


Figure 26. NOVICE versus CRÈME-96 calculations of deposited energy in 75 micron diameter RCC volumes of Si show generally poor agreement at both 2 and 50 micron thicknesses.

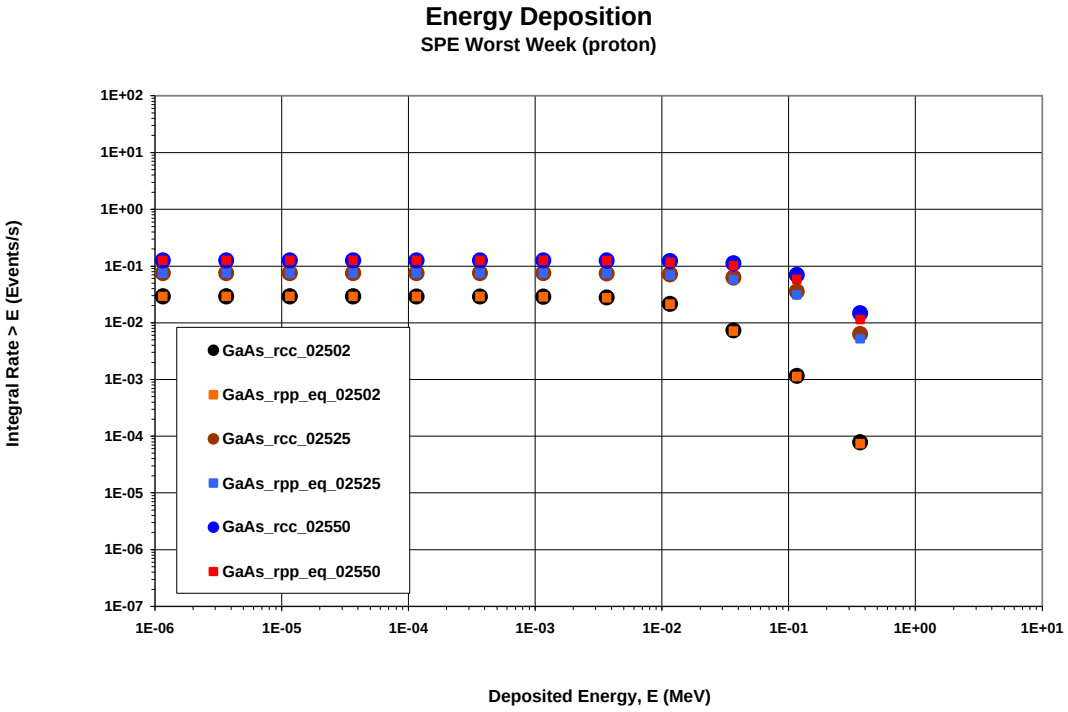


Figure 27. Comparisons of IRCC versus IRPP proton energy deposition distributions in GaAs are made for cylinders with 25 micron diameter and heights of 2, 25, and 50 microns. Corresponding aspect ratios are 12.5, 1.0, and 0.5.

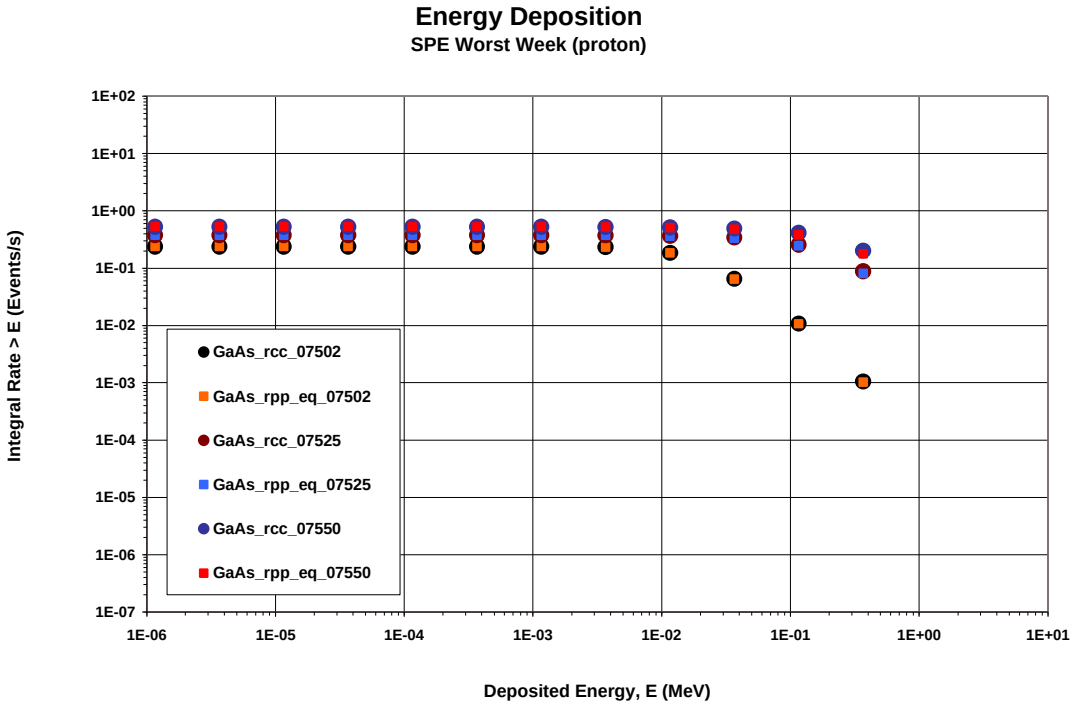


Figure 28. Comparisons of IRCC versus IRPP proton energy deposition distributions in GaAs are made for cylinders with 75 micron diameter and heights of 2, 25, and 50 microns. Corresponding aspect ratios are 37.5, 3.0, and 1.5.

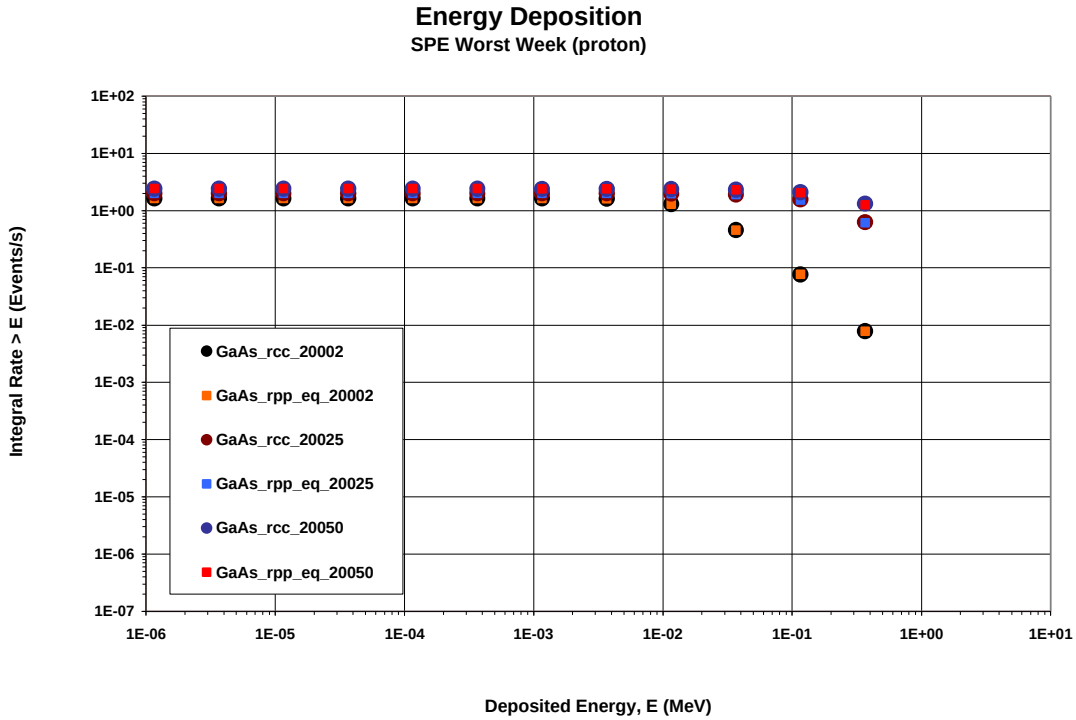


Figure 29. Comparisons of IRCC versus IRPP proton energy deposition distributions in GaAs are made for cylinders with 200 micron diameter and heights of 2, 25, and 50 microns. Corresponding aspect ratios are 100, 8.0, and 4.0.

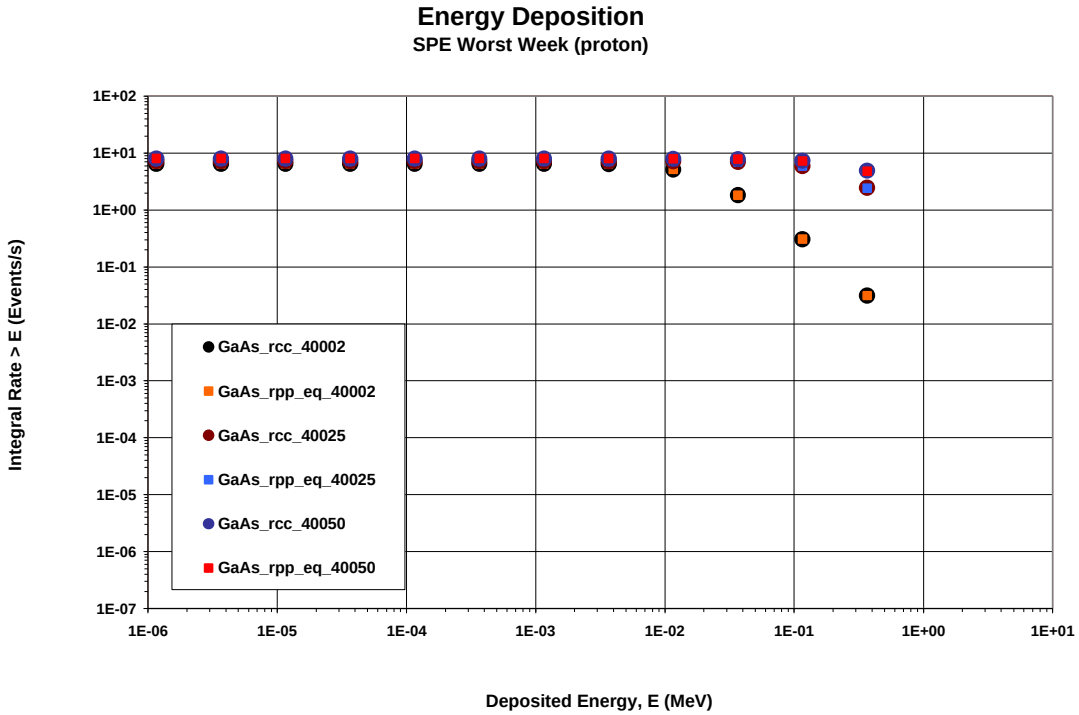


Figure 30. Comparisons of IRCC versus IRPP proton energy deposition distributions in GaAs are made for cylinders with 400 micron diameter and heights of 2, 25, and 50 microns. Corresponding aspect ratios are 200, 16.0, and 8.0.

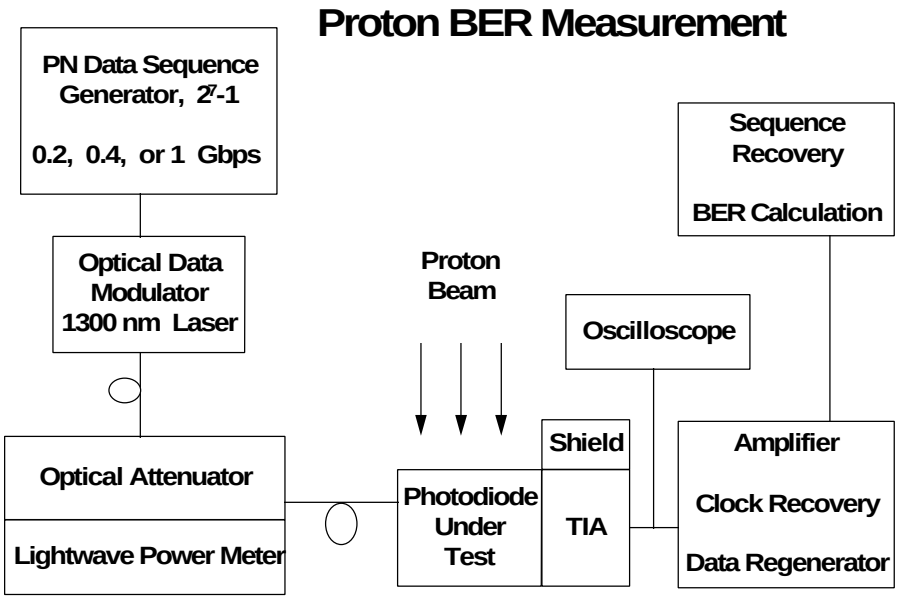


Figure 31. Typical setup for *in-situ* testing of operating FOL (after [8]).

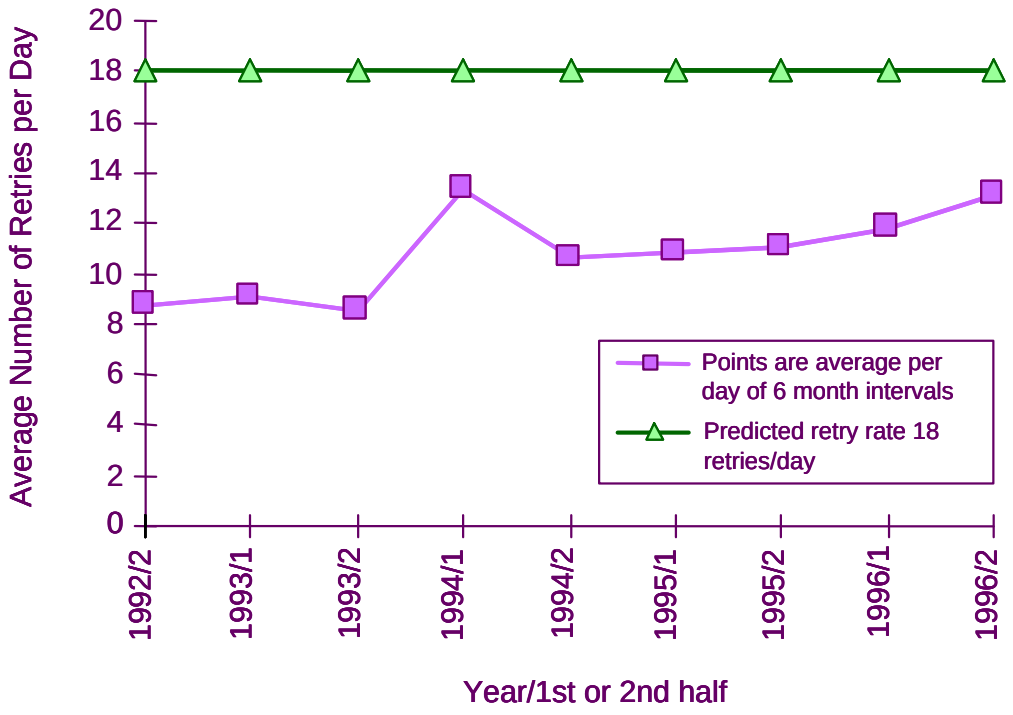


Figure 32. Predicted and measured event rates for the SAMPEX MIL-STD-1773 data bus show agreement to within a factor of 2 (after [11]).

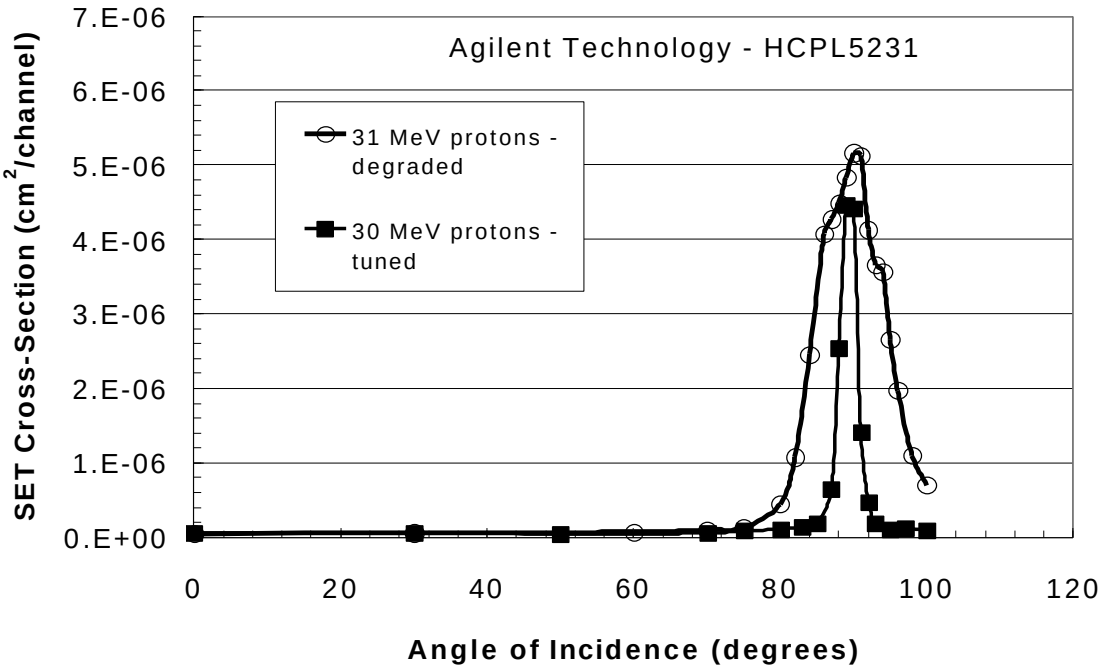


Figure 33. Optocoupler error cross sections for the HCPL5231 show dramatic differences for tuned versus degraded beam energies, presumably due to angular dispersion of the scattered protons as their energy is degraded (after [18]).